ELSEVIER

Physics of the Earth and Planetary Interiors 103 (1997) 207–245

PHYSICS OF THE EARTH AND PLANETARY INTERIORS

A database for the Matuyama–Brunhes magnetic reversal

J.J. Love [a,*], A. Mazaud [b]

[a] *Department of Earth Sciences, The University of Leeds, Leeds LS2 9JT, UK*
[b] *Centre des Faibles Radioactivités, Laboratoire Mixte CNRS-CEA, 91198 Gif-sur-Yvette, Cedex, France*

Received 12 August 1996; received in revised form 28 April 1997; accepted 9 May 1997

Abstract

We present a paleomagnetic database, designated MBD97, comprising sedimentary and lava data for the Matuyama–Brunhes reversal transition field. Using criteria regarding suitability of the rock samples, measurement methods and temporal resolution of the data, we consider 62 different studies of the Matuyama–Brunhes reversal; of these, only 11 satisfy our selection criteria: four lava sites, one loess site, three shallow-marine sedimentary sites, and three deep-ocean sedimentary sites. We discuss our reasons for accepting or disguarding each candidate data set. We investigate the distribution of transitional virtual geomagnetic poles (VGPs); they fall along American and Asian–Australian longitudes. The spatial and temporal complexity of the data indicate that the transitional field was almost certainly nonaxisymmetric and nondipolar. The directional transition of the Matuyama–Brunhes reversal took ~2300–5000 years, during which time the surface intensity fell to ~10–20% of its pre- and post-transitional value. We do not find any systematic bias due to site distribution or inclination shallowing, although the errors in the data do vary over the duration of the reversal. MBD97 is a small database, but it has a fairly good geographic distribution and is suitable for studies of the Matuyama–Brunhes transition, nonetheless, it is clear that further analysis of transitions will benefit from a continued program of data collection and analysis. The data in MBD97 are listed. © 1997 Elsevier Science B.V.

Keywords: Paleomagnetic database; Matuyama–Brunhes reversal transition field; Lava sites; Loess sites; Shallow-marine sediment; Deep ocean sediment

1. Introduction

The occasional reversal of the earth's magnetic field is one of the most perplexing phenomena in geophysics. Reversals occur with remarkable irregularity: the time between reversals can vary from hundreds of thousands to tens of millions of years, with the actual duration of a reversal, defined in terms of field directions, occurring over a relatively more brief period of thousands to tens of thousands of years. In contrast to the temporal dependence of reversals, the spatial geometry of the *reversal transition field* (RTF) displays a tantalizing regularity, maps of *virtual geomagnetic poles* (VGPs), corresponding to paleomagnetic directions at each site, tend to fall along two separate paths: one along longitudes of the Americans and the other along longitudes of Asia–Australia (Clement, 1991; Laj et al., 1991). However, the significance of these observations is controversial (Valet et al., 1992; Egbert, 1992; Langereis et al., 1992; McFadden et al., 1993; Prévot and Camps, 1993; Barton and McFadden, 1996).

* Corresponding author.

PII S0031-9201(97)00034-4

What is clear is that further improvement in our understanding of the reversal process will depend on the analysis of quality data. But since the earth spends only a few percent of its time reversing, paleomagnetic samples which record the RTF are relatively rare. Transitional data come from sedimentary and lava rock samples which record the magnetic field in different and complimentary ways. Paleomagnetic sedimentary samples are collected from lake bottoms, shallow-marine environments, ocean cores and wind-blown loess. Unfortunately, judging the reliability of these different data is often difficult; sedimentary data may be affected by temporal smoothing of the magnetic signal, variations in sedimentation rate, sediment compaction, and variations in the magnetic properties and chemistry of the sediments with stratigraphic depth. On the other hand, paleomagnetic lava samples can provide much more reliable records of the magnetic field direction, and provide the only record of absolute intensity, but since volcanoes erupt sporadically, paleomagnetic lava data are usually a highly discontinuous record of geomagnetic field variations.

Fuller et al. (1979), Athanassopoulos (1993) and Prévot and Camps (1993) have compiled paleomagnetic directional databases covering multiple reversals. More recently, Hartl and Tauxe (1996) and Camps and Prévot (1996) extended these compilations to include intensity data as well, while Singer and Pringle (1996) and Tauxe et al. (1996) have analyzed a number of records in order to better determine the date of the most recent reversal, the Matuyama–Brunhes (0.78 Ma). Here, we report our own survey of the literature for records of the Matuyama–Brunhes. The available transitional data come from a variety of published sources, written by numerous investigators over the last three decades. The data are of widely varying quality, and thus, some discrimination is necessary. We review the data and select a subset which satisfies certain criteria for a database, designated MBD97.

2. Matuyama–Brunhes reversal records

Beginning with a few definitions, an *intermediate* direction (I) is an inclination–declination pair with a corresponding VGP between latitudes $\pm 55°$. Some investigators have used different cut-offs for defining intermediate directions: Prévot and Camps (1993) and Quidelleur et al. (1994) adopted $\pm 60°$. In Fig. 1, we show the geographic variation of VGP latitude for the time-averaged (2.5 Ma) paleomagnetic field model of Gubbins and Kelly (1993) and for the modern field model of Bloxham and Jackson (1992). Note that the paleomagnetic field model shows much less departure from an axial dipole than the modern field model; the lowest VGP latitude is $\sim 82°$ for the paleo field, as compared to $\sim 55°$ for the modern field. The lower VGP latitudes of the modern field are due to nonaxial dipole structure, much of which is secular variation and is averaged-out over the long time scales assumed in constructing the paleomagnetic field model. Johnson and Constable (1996), seeking to exclude intermediate data, used a $\pm 55°$ VGP latitude cut-off in their compilation of interreversal paleomagnetic data. Clearly, because VGP latitude is a function of site location and field morphology, defining an intermediate direction is somewhat arbitrary. In this compilation of intrareversal paleomagnetic data, we define a direction as *normal* (N) if it has a VGP latitude above 55° and *reverse* (R) if it has a VGP latitude below $-55°$. A direction is defined as *transitional* (T) if it is intermediate and part of a polarity transition, either R → N or N → R, being bounded by N (R) and R (N) directions. A direction is defined as *excursional* if it is intermediate but not part of a polarity transition, being bounded by N (R) and N (R) directions. The Matuyama–Brunhes polarity transition is R → N.

To study the rapid and complicated changes in the magnetic field which occurred during the Matuyama–Brunhes transition, we seek a database consisting of intensity, inclination and declination (F, I, D). The data should come from a globally well-distributed set of sites and each paleomagnetic record should pass minimal criteria. To establish selection criteria, we follow the published advice given in papers concerned with data collection (Valet et al., 1988; Clement, 1994), and we follow the example of Johnson and Constable (1996). The criteria are primarily concerned with the dating of the data, completeness in terms of (F, I, D), the measurement and demagnetization methods, mineralogical variations of the rock samples, sedimentation rate, temporal resolution, consistency with data from

neighboring sites, noise content and the paleomagneticist's faith in his own data. The details of our selection criteria are given in Appendix A. A discussion of each candidate reversal record is given in Appendix B; for the records which are not accepted, we indicate which selection criteria are not satisfied. The results of our selection are summarized in Table 1. Of the 62 candidate data sets, only 11 satisfy our

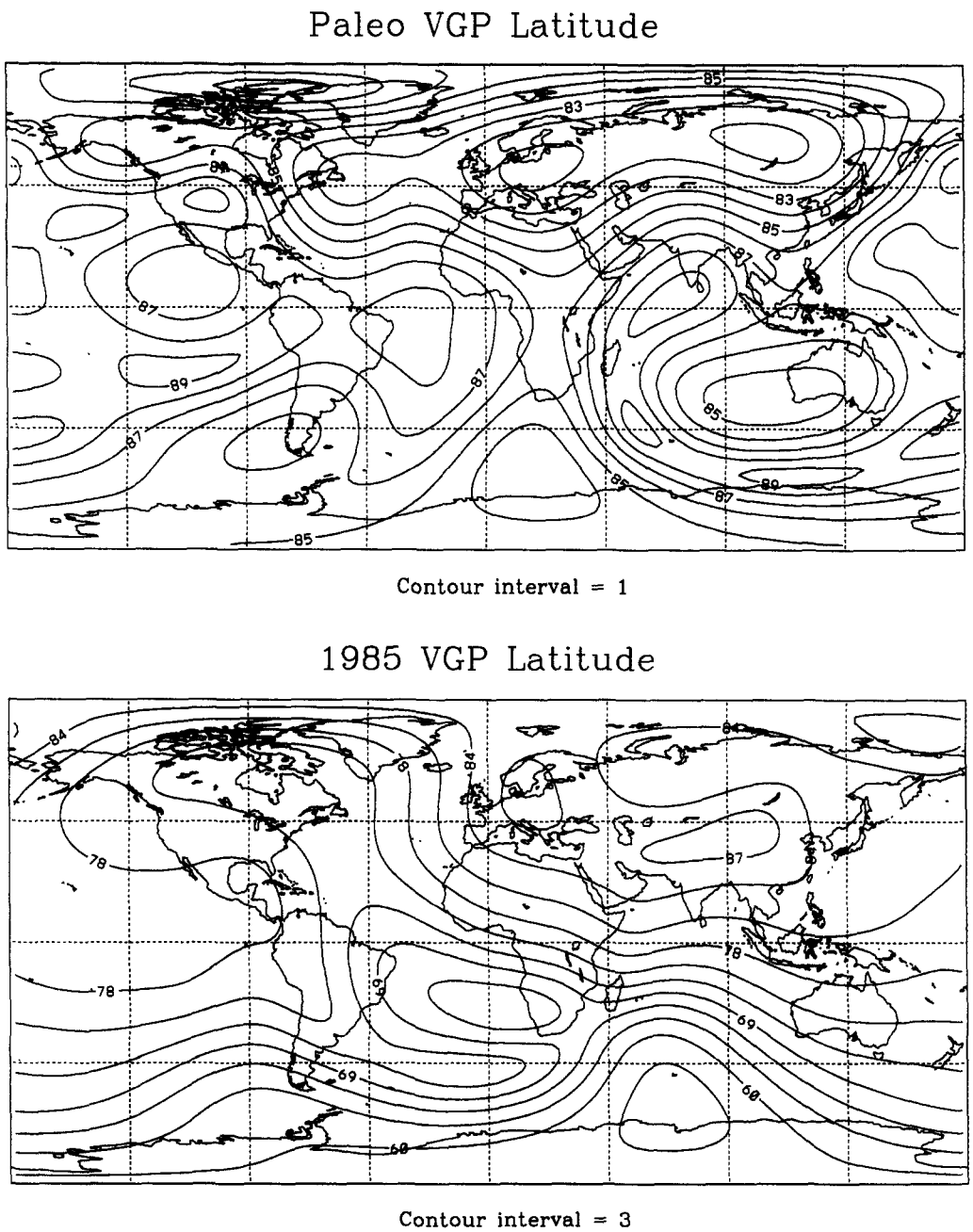

Fig. 1. Contour map of VGP latitude for time-averaged (2.5 Ma) paleomagnetic field model of Gubbins and Kelly (1993) and of the modern field model of Bloxham and Jackson (1992) for 1985. Contour units are in degrees.

Table 1
Summary of Matuyama–Brunhes records

Matuyama–Brunhes														
Locality	Name	Lat. (° N)	Long. (° E)	Type	Data	Sed. rate (cm/kyr)	Demag.	Step	Min.	Res.	Con.	$\langle \alpha_{95} \rangle$	Date	Author judge
Iceland	NU	63.5	340.3	lava	*I, D, F*	–	AF	Y		N		4.8		Kristjánsson et al. (1988)
Iceland	Tjörnes	66.0	342.8	lava	*I, D*	–	AF	Y		Y		4.8	N	Kristjánsson et al. (1988)
Tahiti	**Punaruu**	**−17.7**	**210.3**	**lava**	***I, D, F***	–	**T, AF**	**Y**		**Y**		**4.4**		Chauvin et al. (1990)
China	**Tongjing**	**37.8**	**120.8**	**lava**	***I, D, F***	–	**T**	**Y**		**Y**		**5.8**		Zhu et al. (1991)
Hawaii	**Haleakala**	**20.7**	**203.7**	**lava**	***I, D***	–	**AF**	**Y**		**Y**				Baksi et al. (1992)
Chile	**Tatara**	**−36.0**	**289.0**	**lava**	***I, D***		**T, AF**	**Y**		**Y**		**13.9**		Brown et al. (1994)
Canary	La Palma LL	28.6	342.2	lava	*I, D, F*	–	T, AF	Y		N		7.9		Quidelleur and Valet (1996)
Canary	La Palma LS	28.6	342.2	lava	*I, D, F*	–	T, AF	Y		N		6.8	N	Quidelleur and Valet (1996)
California	Tecopa 1	36.0	243.7	lake	*I, D*	4.5–5.0	AF, U	Y	Y	Y	N	12.6		Hillhouse and Cox (1976)
California	Tecopa 2	36.0	243.7	lake	*I, D, F*	4.5–5.0	T, AF, U	Y	Y	Y	N			Valet et al. (1988)
California	Tecopa 3	35.0	243.0	lake	*I, D*	4.5–5.0	T, AF, U	Y	N		N			N Larson and Patterson (1993)
California	Bishop A1	37.4	241.0	lake	*I, D*	25	T, AF	Y	N	N		32.4		N Liddicoat (1993)
California	Bishop A2	37.4	241.0	lake	*I, D*	25	T, AF	Y	N	N		15.8		N Liddicoat (1993)
California	Bishop A3	37.4	241.0	lake	*I, D*	25	T, AF	Y	N	N		52.9		N Liddicoat (1993)
Czech	Červený Kopec 1	49.3	16.5	loess	*I, D*		N	N	N				N	Bucha (1970)
Czech	Červeuý Kopec 2	49.3	16.5	loess	*I, D*		AF	N	N					Kočí et al. (1974)
Czech	Suchdol	50.2	14.3	loess	*I, D*		AF	N	N					Kočí et al. (1974)
Germany	Briiggen	51.3	6.3	loess	*I, D*		N	N	N					Kočí and Šibrava (1976)
Germany	Regansburg	49	12.1	loess	*I, D*		N	N	N					Kočí and Šibrava (1976)
Austria	Krems	48.5	15.6	loess	*I, D*		N	N	N					Kočí and Šibrava (1976)
China	Xifeng 1	36.0	108.0	loess	*I, D*	10.0	T	Y	F	Y	N			Sun et al. (1993)
China	Xifeng 2	36.0	108.0	loess	*I, D, F*	10.0	T	Y	Y	N	Y	10.4		Zhu et al. (1993)
China	**Weinan**	**34.2**	**109.2**	**loess**	***I, D, F***	**9.3**	**T**	**Y**	**Y**	**Y**	**Y**			Zhu et al. (1994)
Japan	Boso Y	35.2	140.2	marine	*I, D, F*	370	AF	N	N	Y				Niitsuma (1971)
Japan	**Boso H**	**35.2**	**140.2**	**marine**	***I, D, F***	**220**	**AF**	**Y**	**Y**	**Y**	**Y**	**19.0**		Okada and Niitsuma (1989)
Japan	**Boso C**	**35.2**	**140.2**	**marine**	***I, D, F***	**183**	**AF**	**Y**	**Y**	**Y**	**Y**	**13.4**		Okada and Niitsuma (1989)
New Zealand	**Wanganui**	**−40.0**	**175.0**	**marine**	***I, D***	**10's**	**T**	**Y**	**Y**	**Y**				Turner and Kamp (1990)
Pacific	Papagayo	14.8	240.1	ocean	*I, D, F*	0.2	AF	Y						Harrison and Somayajulu (1966)
Pacific	KH70-2-5	38.4	189.9	ocean	*I, D, F*	0.1	N	N	N					Kawai et al. (1973)
Pacific	KH73-4-7	2.7	164.8	ocean	*I, D, F*	0.6	AF	Y	Y					Kawai et al. (1977)
Pacific	KH73-4-8	−1.5	167.6	ocean	*I, D, F*	0.6	AF	Y	Y					Kawai et al. (1977)
Pacific	RC10-167	33.4	150.4	ocean	*I, F*	2.1	AF	Y	Y	N				Kent and Opdyke (1977)

Pacific	RC9-114	−33.4	195.0	ocean	*I, D*	1.2	AF	Y	N	Y		Clement and Kent (1984)
Pacific	RC9-119	−23.2	188.4	ocean	*I, D*	0.7	AF	Y	N	N		Clement and Kent (1984)
Pacific	RC10-182	45.4	177.5	ocean	*I, D*	1.1	AF	Y	N	Y		Clement and Kent (1984)
Pacific	RC15-21	1.5	227.0	ocean	*I, D*	1.0	AF	Y	N	Y		Clement and Kent (1984)
Pacific	V20-104	37.2	181.9	ocean	*I, D*	0.8	AF	Y	N	Y		Clement and Kent (1984)
Pacific	V20-107	43.4	181.1	ocean	*I, D*	0.7	AF	Y	N	Y	N	Clement and Kent (1984)
Pacific	V20-108	45.4	180.8	ocean	*I, D*	1.1	AF	Y	N	Y	N	Clement and Kent (1984)
Pacific	K78-10-19	9.0	189.8	ocean	*I, D, F*	1.7	AF	Y	Y	N		Theyer et al. (1985)
Pacific	K78-10-30	18.9	199.6	ocean	*I, D, F*	3.5	AF	Y	Y	N		Theyer et al. (1985)
Pacific	767B	4.8	123.5	ocean	*I, D, F*	7.0–8.0	AF, U	Y	Y	N		Schneider et al. (1992)
Pacific	769A	8.8	121.3	ocean	*I, D, F*	10.0–12.0	AF	Y	Y	N		Schneider et al. (1992)
Pacific	792A	30.4	140.4	ocean	*I, D, F*	8.1	T, AF	Y	F	N		Cisowski and Koyama (1992)
Pacific	851D	2.8	249.4	ocean	*D, F*	2.0	AF	Y	Y			Valet and Meynadier (1993)
Pacific	803B	2.3	160.3	ocean	*I, D, F*	1.0	T, AF	Y	Y	Y		Hartl and Tauxe (1996)
Pacific	804C	1.0	161.4	ocean	*I, D, F*	1.0	T, AF	Y	Y	Y		Hartl and Tauxe (1996)
Pacific	805B	1.1	160.3	ocean	*I, D, F*	2.0	T, AF	Y	Y	Y		Hartl and Tauxe (1996)
Atlantic	V30-45	6.2	340.4	ocean	*I, D*	0.5	AF	Y	N	N		Clement and Kent (1984)
Atlantic	606A	37.3	324.5	ocean	*I, D, F*	2.8–3.2	AF, U	Y	N		N	Clement and Kent (1986)
Atlantic	607A	41.0	327.0	ocean	*I, D, F*	4.3–5.0	AF, U	Y	N			Clement and Kent (1986)
Atlantic	**609B**	**49.9**	**335.8**	**ocean**	***I, D, F***	**5.9–8.3**	**AF**	**Y**	**Y**	**Y**		Clement and Kent (1986)
Atlantic	610B	53.2	341.1	ocean	*I, D, F*	5.7–6.1	AF	Y	N		N	Clement and Kent (1986)
Atlantic	610C	53.2	341.1	ocean	*I, D, F*	5.6	AF	Y	N		N	Clement and Kent (1986)
Atlantic	642B	67.2	2.9	ocean	*I, F*	4.0	AF	Y	Y	N	Y	Schönharting et al. (1989)
Atlantic	642C	67.2	2.9	ocean	*I, F*	4.0	AF	Y	Y	N	Y	Schönharting et al. (1989)
Atlantic	643A	67.7	1.0	ocean	*I, F*	2.0	AF	Y	Y	N	Y	Schönharting et al. (1989)
Atlantic	644A	67.0	4.5	ocean	*I, F*	10.0	AF, U	Y	Y		Y	Schönharting et al. (1989)
Atlantic	659C	18.1	339.0	ocean	*I, D, F*	2.7–3.1	T, AF	Y	Y	N		Valet et al. (1989)
Atlantic	**664D**	**0.1**	**336.7**	**ocean**	***I, D, F***	**3.6–4.4**	**T, AF**	**Y**	**Y**	**Y**		Valet et al. (1989)
Atlantic	665B	0.0	336.7	ocean	*I, D, F*	1.5	T, AF	Y	Y	N		Valet et al. (1989)
Indian	**V16-58**	**−46.0**	**30.0**	**ocean**	***I, D, F***	**4.0**	**AF**	**Y**	**Y**	**Y**		Clement and Kent (1991)

Data: (*I*) inclination, (*D*) declination, (*F*) intensity. Demag.: type of demagnetization used in cleaning samples, (T) thermal, (AF) alternating field, (U) unsuccessful removal of overprint, (N) no demagnetization. Step: (Y) step-wise demagnetization was used, (N) no step-wise demagnetization. Min.: (Y) passes mineralogical criterion, (N) no mineralogical study, (F) fails mineralogical criterion. Res.: (Y) satisfies resolution criterion, (N) does not satisfy resolution criterion. Con.: (Y) obviously consistent with neighboring record, (N) obviously inconsistent with neighboring record. Date: (N) flows were not dated. $\langle \alpha_{95} \rangle$: average precision parameter for entire data set. Author judge: (N) author finds data unacceptable. Note: the sites accepted into MBD97 are represented in bold font.

selection criteria: four lava sites, one loess site, three shallow-marine sedimentary sites and three deep-ocean sedimentary sites. From these selected sites, there are 650 directions, 170 of which are intermediate, and of these, 73 are transitional; there are eight absolute intensity measurements and 380 relative

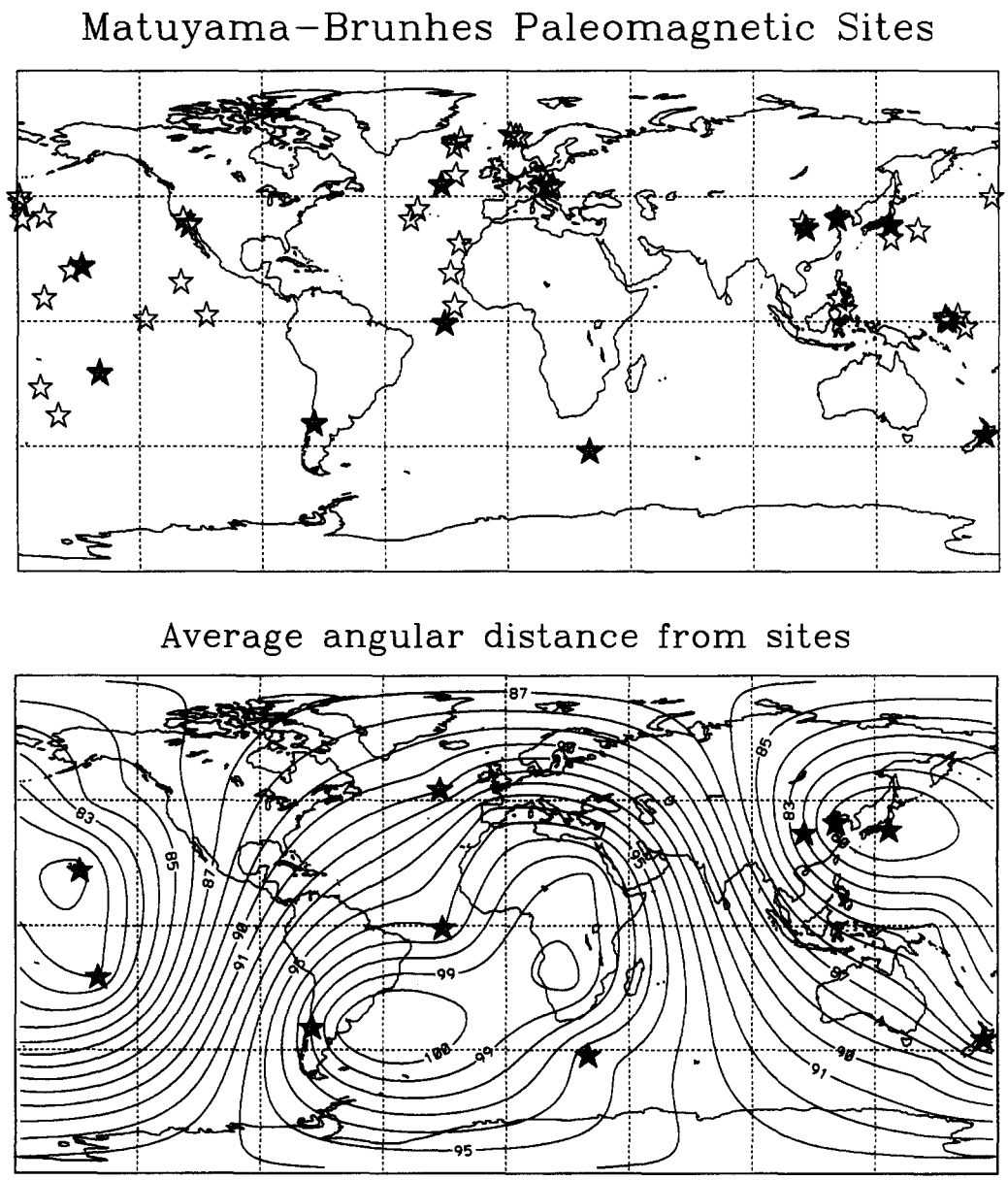

Fig. 2. The geographic distribution of the 62 candidate sites and contour plot of the average angular distance form the accepted data sites. Solid star (*openstar*) indicates a site (not) included in this compilation. For the contour plot, the two Boso sites in Japan are counted as one site. The area least well covered area is the southern Atlantic and the best covered area is the northern Pacific. Note that perfectly uniform coverage would correspond to a contour level of 90°.

intensity measurements. Although the site distribution is sparse, it is fairly uniform (see Fig. 2). In Appendix C, we list the data of MBD97.

3. Discussion

MBD97 allows us to address a number of issues concerning the nature of the transitional field, some of which are well established and others of which remain controversial. Beginning with the less contentious points, it is fairly well documented that a field reversal is initiated by a gradual diminution in intensity, followed by a relatively rapid change in field direction and a subsequent increase in intensity (Lin et al., 1994). The decrease in transitional intensity at the earth's surface could be due to a combination of an actual decrease in the field intensity at the core surface and a shift in field energy from long wavelength (low spherical harmonic degree) ingredients to short wavelength (higher spherical harmonic degree) ingredients, thereby causing an apparent decrease in intensity at the earth's surface due to geometric attenuation. However, the fact that the intensity decrease occurs before the field directions change is probably indicative of at least some real decrease in core surface field intensity. MBD97 shows that the directional transition of Matuyama–Brunhes took ~ 2300–5000 years, during which the surface field intensity fell to ~ 10–20% of the pre- and post-transitional field strength. Following Dagley and Wilson (1971), we plot the relative intensity versus VGP latitude (see Fig. 3).

The transitional data of MBD97 indicate that the Matuyama–Brunhes RTF was nonaxisymmetric and nondipolar. Laj et al. (1991) plotted the VGP paths from a number of sedimentary records for the last several reversals. What emerged from their analysis was an apparent preference for the transitional VGP to fall along two paths, one located along the Americans and the other along Asia–Australia. It has been noted that such an effect may be due to a nondipolar transitional field (Clement, 1991; Gubbins and Coe, 1993); indeed, MBD97 has intermediate VGPs which tend to fall along the American and Asia–Australian paths (see Figs. 4 and 5).

However, the significance of observations such as these has been disputed. The preferred paths may be merely an artifact of a poor distribution of sites (Valet et al., 1992) combined with a bias inherent to the VGP mapping (Egbert, 1992) causing VGPs to fall along longitudes $\pm 90°$ from site longitudes. This effect could be enhanced by inclination shallowing of the sedimentary records (Barton and McFadden, 1996), particularly during weak transitional field strengths. It has also been suggested that the preferred paths may be an artifact of post-depositional smoothing of the sedimentary data (Langereis et al., 1992), although Zhu et al. (1994) have noted that this is unlikely because of evident rapid directional changes in some transitional records.

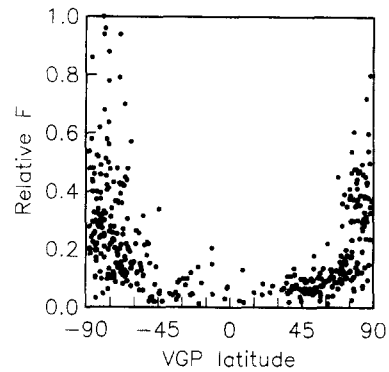

Fig. 3. Relative intensity versus VGP latitude. The intensities have been normalized so that the pre- and post-transitional data vary with site latitude like that of an axial dipole.

To check for possible bias due to site distribution, we consider the VGP longitude minus site longitude (see Fig. 6). Note that the longitudinal difference shows no obvious tendency to fall along longitudes $\pm 90°$ from site longitudes, even during periods of weak field strength or low VGP latitude. And from inspection of the histograms in Fig. 6, it is clear that the VGPs, rather than falling along longitudes $\pm 90°$ from site longitudes, tend to fall along longitudes closer to the site longitudes. Such an effect is consistent with a nondipolar transitional field where the local magnetic field vector simply points towards (away from) the nearest concentration of negative (positive) flux (Gubbins and Coe, 1993). We conclude that the tendency for VGPs from MBD97 to fall along preferred longitudes is not the result of bias introduced by a poor distribution of sites.

Next, we check for inclination shallowing. Instead of displaying the data by proxy VGPs, it is more

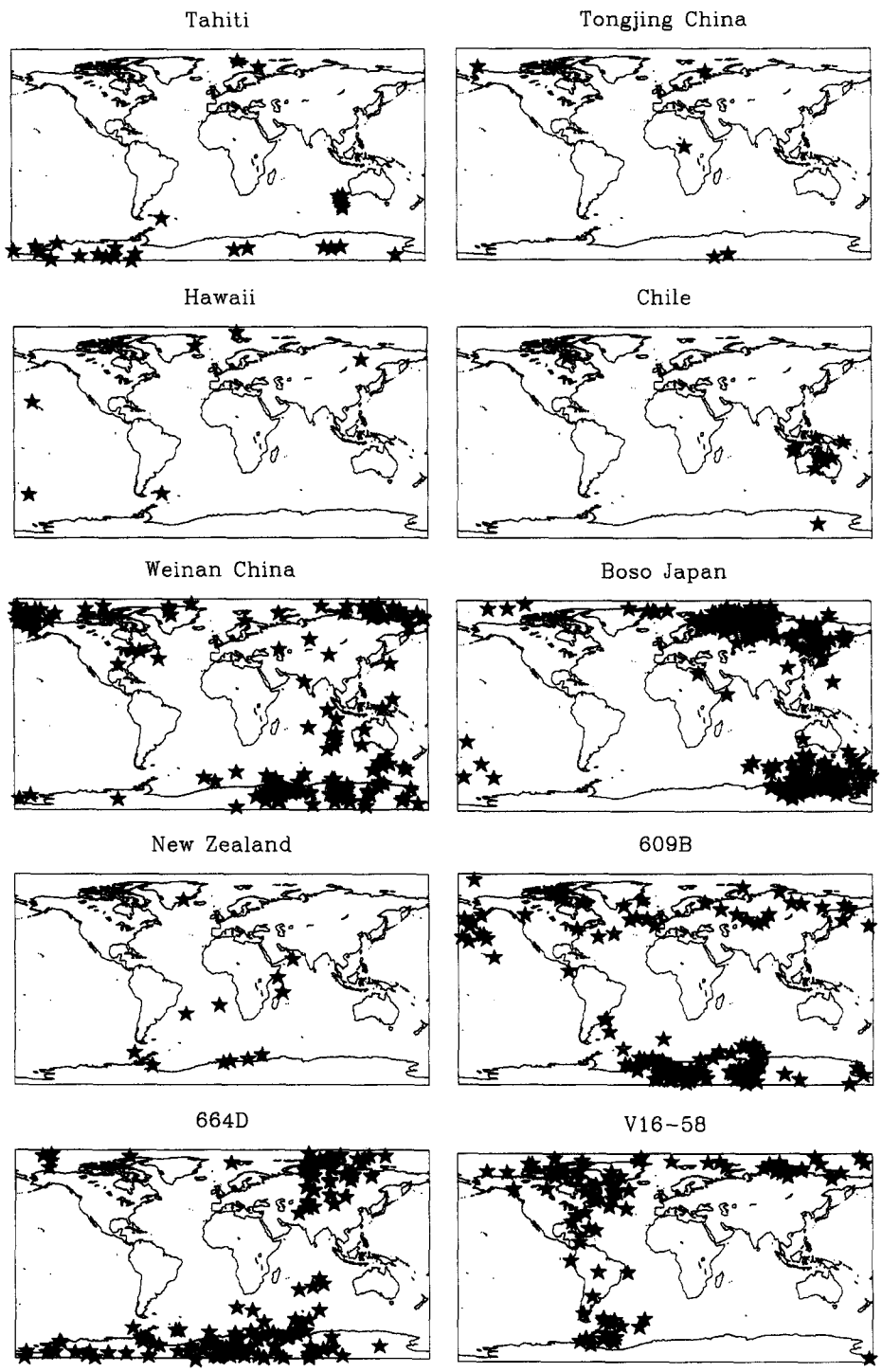

Fig. 4. VGPs for MBD97 with $\alpha_{95} < 30°$ for each site. Note that the two Boso Japan sites have been plotted together.

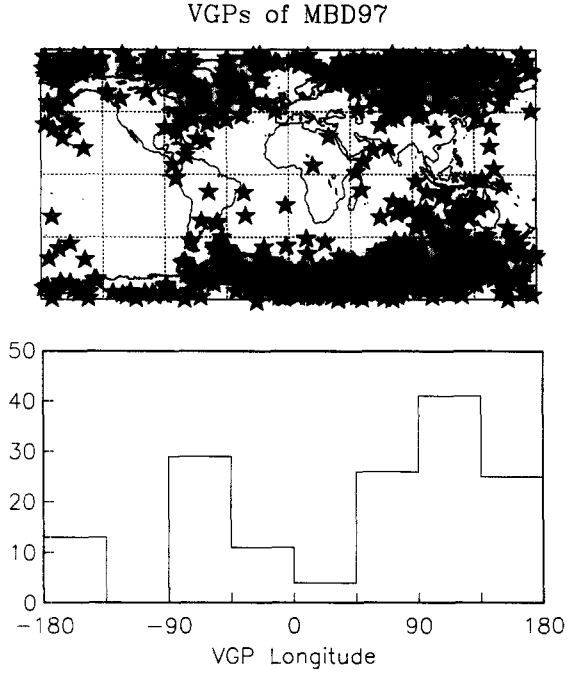

Fig. 5. Geographic distribution of all VGPs for MBD97 with $\alpha_{95} < 30°$, together with histogram showing the longitudinal distribution of the intermediate VGPs (those with latitudes between $\pm 55°$).

straightforward to simply display data anomalies. We define an inclination anomaly $A(I)$ as the deviation from the inclination of an axial dipolar field,

$$A(I) = I - \tan^{-1}(2\tan(\lambda_{\text{Site}})) \text{ for } \lambda_{\text{VGP}} > 0°,$$
$$A(I) = I + \tan^{-1}(2\tan(\lambda_{\text{Site}})) \text{ for } \lambda_{\text{VGP}} < 0°, \quad (1)$$

where λ_{site} and λ_{VGP} are the site latitude and VGP latitude, respectively. Thus, the inclination anomaly is negative if there is shallowing and positive if there is deepening. Similarly, we define a declination anomaly $A(D)$,

$$A(D) = D + n360° \text{ for } \lambda_{\text{VGP}} > 0°,$$
$$A(D) = D - 180° + n360° \text{ for } \lambda_{\text{VGP}} < 0°, \quad (2)$$

where n is an integer which is adjusted so that $-180° < A(D) < 180°$.

Using these definitions in Fig. 7, we plot the intensity versus inclination and declination anomalies for the sedimentary data. Note that the scatter of the anomalies increases with decreasing field intensity, consistent with a relatively weak nonaxisymmetric nondipolar transitional field. Interestingly, there is no obvious inclination shallowing with decrease in field intensity. In fact, if anything, the situation is slightly the opposite, namely inclination deepening, something we interpret as part of the secular variation. Similarly, the plots of VGP latitude versus inclination anomaly and the histograms of the anomalies all demonstrate a lack of inclination shallowing in the sedimentary data of MBD97. This point is emphasized in Table 2, where we display $\langle A(I)\rangle$ and $\langle A(D)\rangle$, the average inclination and declination anomalies, respectively, and $\sigma_{A(I)}$ and

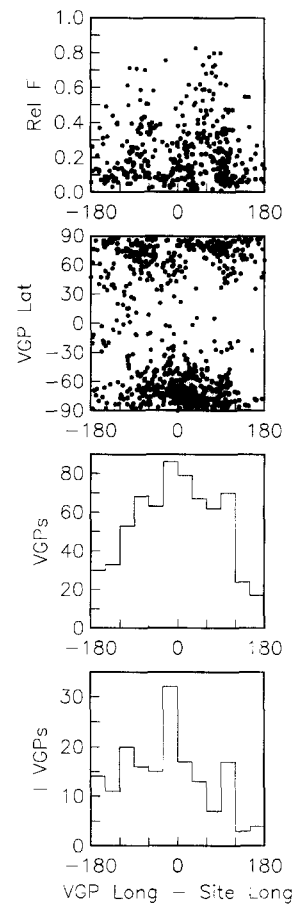

Fig. 6. Relative intensity, VGP latitude and binned distributions of VGPs versus VGP longitude minus site longitude. The intensities have been normalized so that the pre- and post-transitional data vary with site latitude like that of an axial dipole. I denotes intermediate VGPs only (those with latitudes between $\pm 55°$). Note that the histograms do not show any obvious tendency for the VGPs to fall along longitudes $\pm 90°$ from the site longitude.

$\sigma_{A(D)}$, the corresponding standard deviations; notice that $\langle A(I)\rangle$ is positive for the sedimentary data. We conclude that the apparent tendency for VGPs from MBD97 to fall along preferred longitudes is not the result of systematic errors in the data caused by inclination shallowing of the sedimentary records.

Another issue which we need to address is the degree of serial correlation of the sedimentary data. Because the degree of alignment of magnetic particles in sediment depends on the field strength, it might be expected that the temporal scatter of the inclinations will increase with decreasing intensity,

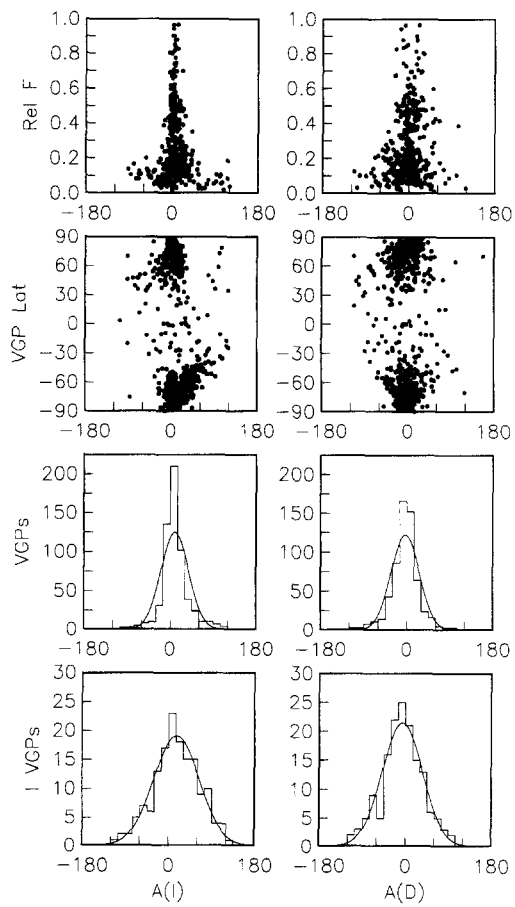

Fig. 7. Relative intensity, VGP latitude and binned distributions of VGPs versus inclination anomaly, $A(I)$, and declination anomaly, $A(D)$, each measured in degrees, for all sedimentary data. I denotes intermediate VGPs only (those with latitudes between $\pm 55°$). Note that the inclination anomaly is, on average, positive, indicating slight inclination deepening of the data.

Table 2
Average inclination anomaly, $\langle A(I)\rangle$, and declination anomaly, $\langle A(D)\rangle$, for all sedimentary data, together with their standard deviations, $\sigma_{A(I)}$ and $\sigma_{A(D)}$. I denotes intermediate data only

I and D anomaly properties				
Data	$\langle A(I)\rangle$	$\sigma_{A(I)}$	$\langle A(D)\rangle$	$\sigma_{A(D)}$
All sed. data	9.5°	29.0°	−3.6°	29.6°
I sed. data	16.3°	47.7°	−6.5°	42.4°

and the temporal scatter of the declinations will increase with either a decrease in field intensity or with the field approaching vertical. It may also be the case that field directions change more rapidly during periods of weak field intensity, in which case temporal scatter may be, at least partially, due to rapid secular variation. We can measure the temporal scatter, normalized by intensity, by measuring the excursion from a temporal running average. For each stratigraphic level i, we define the quantities

$$\sigma(F)_i = \ln\left(\frac{F_i}{F_0}\right) - \left\langle \ln\left(\frac{F_i}{F_0}\right)\right\rangle,$$
$$\sigma(I)_i = \left(I_i - \langle I_i\rangle\right)\frac{\langle F_i\rangle}{F_0}, \qquad (3)$$
$$\sigma(D)_i = \left(D_i - \langle D_i\rangle\right)\frac{\langle H_i\rangle}{F_0}.$$

F_0, is used for normalization of the relative intensities; we define F_0 so that F/F_0, for the pre- and post-transitional data, varies with site latitude like that of an axial dipole. The horizontal intensity is $H = F\cos(I)$. The quantity $\langle \cdots \rangle$ denotes a three-point running average of vertically adjacent stratigraphic levels.Note that $\sigma(I)$ and $\sigma(D)$ are similar to the weighted residuals used in modelling modern field data (Lowes, 1975).

The quantities given in Eq. (3) are plotted in Fig. 8. Insofar as the scatter functions represent our attempt to measure the errors in the data, their nonnormal distributions may indicate that the degree of magnetization acquired by the sediment is not simply proportional to the applied field intensity (this would hardly be surprising). It may also be the case that secular variation not resolved well by the discrete

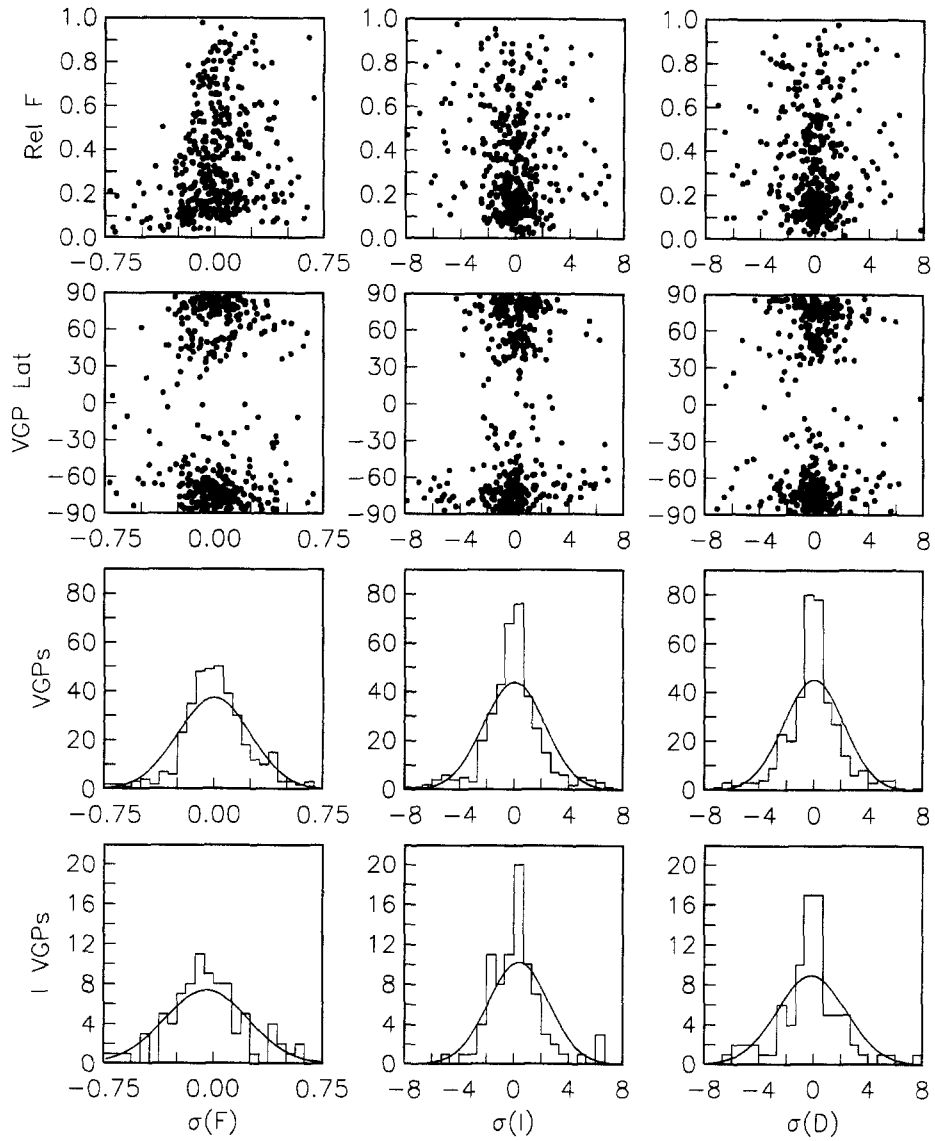

Fig. 8. Relative intensity, VGP latitude and binned distributions of VGPs versus intensity scatter, $\sigma(F)$, inclination scatter, $\sigma(I)$, and declination scatter, $\sigma(D)$, for all sedimentary data. Both $\sigma(I)$ and $\sigma(D)$ are measured in degrees. I denotes intermediate VGPs only (those with latitudes between $\pm 55°$).

sampling of the sediments, especially during periods of weak field intensity when the secular variation may be very rapid, is at least partially responsible for the nonnormal form of the distributions shown in Fig. 8. Of course, from the simple analysis employed here, we have no way of distinguishing between these two possibilities. Nonetheless, if we were to ignore the few outliers near the tails of the distributions, then they might be approximated better as normal. We suggest that a reasonable tolerance within which to fit the directions, should this be desired, is ~ 1–$2°$, with the inclination weighted proportional to total intensity and declination weighted proportional to horizontal intensity. Likewise, noting that the intensity scatter is roughly log-normal, we suggest a tolerance for the intensities of ~ 10–20%.

4. Conclusions

Whether or not the transitional VGPs are confined to, preferred longitudes remains controversial. MBD97 is obviously a fairly small database, constituting what we believe is the best available data recording the Matuyama–Brunhes transition, nonetheless, it appears to show confinement and we have shown that this result appears to be fairly robust. The tendency for transitional VGPs to fall along preferred longitudes probably indicates some underlying nondipolar structure in the transitional data (Gubbins and Sarson, 1994), albeit somewhat difficult to decipher (Gubbins, 1994). Future analysis of transitional data might be made though a multipolar fit to the transitional data. Such a program should treat the data errors appropriately and consider the poorly determined emplacement times of the data at each site.

Acknowledgements

Many people have assisted us with this work by providing us with their data or offering constructive advice. We thank J. Athanassopoulos, A.K. Baksi, L. Brown, B.M. Clement, R. Coe, M. Fuller, D. Gubbins, V. Hsu, C. Laj, J. Pickens, M. Prévot, D.A. Schneider, J. Shaw, G.M. Turner, J.P. Valet and R. Zhu. This work was supported by NERC grant GR3/8238 and the Leverhulme Trust.

Appendix A. Selection criteria

We describe the selection criteria. We follow the published advice given in papers concerned with data collection (Valet et al., 1988; Clement, 1994), and we follow the example of Johnson and Constable (1996). Because there are some questions about the ability of sediments to record reliably the magnetic field during a reversal (Hoffman and Slade, 1986), we require that sedimentary records satisfy several criteria in addition to those applied to lava records. These extra criteria are concerned with the mineralogical homogeneity of the sediments and temporal resolution, and are not necessarily applied appropriately to temporally discontinuous volcanic records.

A.1. Criteria applied to all transitional records

[Date]: Transitional data must belong to the Matuyama–Brunhes transition. In the case of ocean core data, this determination is usually easy: the Matuyama–Brunhes transition is the uppermost nonexcursional transition in the stratigraphic column. In the case of lava samples, at least some samples should have been dated radiometrically or by thermoluminescence.

[Demag.]: The samples, or pilot samples, should have been step-wise alternating field (AF) or thermal (T) demagnetized, and the demagnetization should have yielded a natural permanent magnetization (NRM) with a characteristic field direction which indicates that overprinting has been removed. The demagnetization must have been applied to discrete samples; we do not, for example, accept measurements made of ocean cores by shipboard pass-through magnetometers after bulk demagnetization.

[I and D]: Transitional records must include both inclination (I) and declination (D); we accept relative declination from azimuthally unoriented ocean cores.

[Author Judge]: If the authors themselves conclude that their data are unacceptable then the data are not included in MBD97.

A.2. Additional criterion applied to lava records

[Intensity]: We accept absolute intensity measurements taken from lava samples when the Thellier method was used.

[Resolution]: We require that lava records have at least one transitional direction.

A.3. Additional criteria applied to sedimentary records

[Intensity]: We accept relative intensity measurements from sediments in the form of NRM when it appears that the sediment mineralogy is relatively uniform over stratigraphic height. The uniformity can be measured, for example, by the anhysteretic remanent magnetization (ARM), isothermal remanent magnetization (IRM) or susceptibility (χ); we arbitrarily set an upper limit of 10% for variation of these quantities if unnormalized NRM is to be ac-

cepted as a relative intensity estimate. Otherwise, if the variation is larger, then we require that the intensity be normalized by dividing the NRM by ARM, IRM, or χ.

[Mineral]: In order to insure the relative reliability of data taken from sedimentary samples of different stratigraphic levels, we require that magnetic properties of the samples, as measured by ARM, IRM or χ, should not vary by more than a factor of three over the depth of the transition (Clement, 1994).

[Sed. Rate]: Ocean cores should have a sedimentation rate greater than 3 cm/kyr; lesser rates are unlikely to give sufficient resolution due to smoothing of the magnetic signal (Clement, 1994).

[Resolution]: In the case where the Matuyama–Brunhes RTF is recorded at a site as a single polarity transition, R → N, then we require that the sedimentary paleomagnetic record have three or more consecutive transitional directions preceded by a reverse and followed by a normal direction, RTTTN. On the other hand, some sites record the overall transition as a series of rapid changes of polarity, for example, R → N → R → N. In such a case, we require that at least one of the polarity transitions has at least three consecutive transitional directions, thus, NTTTR is acceptable. Ideally, for the case of multiple polarity fluctuations, we would like to require that each polarity transition be recorded with three intermediate directions, but this is rarely realized. A record with at least one combination of RTTTN or NTTTR gives us some minimal temporal resolution.

A.4. Additional important issues

[Consistency]: Neighboring paleomagnetic records should be consistent. This is obviously a subjective criterion, but in fact, no data are excluded solely on the basis of inconsistency. We find several cases of apparent inconsistency to be obvious by inspection, and we discuss each case individually.

[Scatter]: Samples from the same stratigraphic section must not exhibit excessive scatter. The dispersion in the directions is usually measured by the precision parameter α_{95}, the semi-angle of the cone of 95% confidence centered on the mean direction. Unfortunately, α_{95} is not always reported in the paleomagnetic literature. When α_{95} is available, it might be wise to exclude any data which exceed some chosen cut-off, in their database of nontransitional data, for example, Johnson and Constable (1996) excluded all data for which α_{95} exceeded 30°. We have not excluded any data on the basis of excessive α_{95}, but we note the cases where α_{95} exceeds 30°.

A.5. Future selection criteria

We would like to emphasize that the above criteria should not be regarded as defining an acceptable level for future gathering of reversal data. If we were to compile a wish list of selection criteria, we would, for example, like to require that step-wise demagnetization be performed on all samples (Valet et al., 1988), not just pilot samples (we have accepted pilot sample studies for this compilation), and ideally both AF and T demagnetizations, applied to separate samples, should yield consistent results. We would like to require that all relative intensity measurements be normalized by ARM, IRM or χ. And concerning ocean sedimentary data, we would like to see consistent results come from neighboring cores (much of the ocean sedimentary data accepted in this compilation comes from isolated cores). We have, by necessity, had to compromise some of our ideal expectations with practical realities: if we applied overly strict selection criteria we would have an even smaller database, or, indeed, no database at all. We also realize that time and money are important limiting factors in many paleomagnetic studies. Nonetheless, in the course of completing this work, it became apparent to us that the quality of data has improved dramatically over the last decade, and the clarity with which it is communicated has improved as well. We hope that these trends continue.

Appendix B. Evaluation of data

In the discussion which follows, we indicate the grounds for not accepting data by [n], where n denotes a selection criterion.

B.1. Lava data

B.1.1. Iceland

Kristjánsson et al. (1988) analyzed samples from the Eyjafjöll region of southern Iceland near the Núpakot farm (NU) and from the Tjörnes Peninsula

of northern Iceland. NU samples were oriented, the orientation of the Tjörnes is not reported. A correction for 1° tectonic tilt was applied to the Tjörnes samples. Four to seven samples per lava flow were collected over stratigraphic sections which Kristjánsson et al. believe records the Matuyama–Brunhes transition. Samples were step-wise AF demagnetized up to 25 mT. Thermomagnetic analysis yielded two Curie points for some of the NU samples; all intensity measurements are reported as unnormalized NRM [Intensity]. Although reverse and normal directions were measured in both sites, no transitional directions were measured in the NU flows [Resolution], but several transitional direction were measured in the Tjörnes flows. α_{95} is nearly always below 10°. One flow from NU was dated by the K–Ar method, yielding an age of 0.78 Ma, in accordance with the date of the Matuyama–Brunhes transition. Tjörnes flows could not be dated accurately, thus, it is not certain whether the intermediate directions correspond to the Matuyama–Brunhes transition or an excursion [Date] (see p. 221 of Kristjánsson et al., 1988).

● We do not accept data from Iceland in this compilation.

B.1.2. Tahiti

Chauvin et al. (1990) analyzed samples from Punaruu Valley in Tahiti. Four to eleven oriented samples per lava flow were collected, spanning the duration of the Matuyama–Brunhes RTF. Samples from all flows were step-wise AF demagnetized up to 100 mT, generally 10 mT was sufficient to remove overprint. Duplicate samples from all transitional flows and some normal and reverse flows were step-wise T demagnetized to over 500°C. Susceptibility was measured for most flows, and was found to vary by a factor of ~ 3; we note that three transitional flows were not measured for χ. Absolute intensity was estimated by Thellier method. Five transitional directions were measured. No α_{95} exceeds 30°. Some samples were dated by the K–Ar method, their dates span the Matuyama–Brunhes transition.

B.1.3. Discussion of Tahiti

The Tahitian lava data exhibit a fairly monotonic change in both declination and inclination, with transitional VGPs which cluster off western Australia, similar to the VGP clusters found by Hoffman (1992) from Hawaiian data covering other reversals.

● We accept directional and absolute intensity data from Tahiti in this compilation, obtained from Tables 2 and 3 of Chauvin et al. (1990).

B.1.4. Tonjing, China

Zhu et al. (1991) analyzed samples from the Tongjing basalts, Shandong Province, in northeastern China. The site consists of a layer of loess overlaid by three lava flows and divided by a dyke; multiple oriented samples were taken from each unit, including the baked loess. Each sample was step-wise T demagnetized up to 560°C. Absolute intensity was estimated by Thellier method. Only one transitional direction was measured. No α_{95} exceeds 30°. Only the lowermost baked loess level (LB) was dated, and that by thermoluminescence.

B.1.5. Discussion of Tongjing, China

An estimate of paleomagnetic errors can be made this site. Since the lava reheated the underlying loess, after which the lava and the loess cooled simultaneously, intensity and directions extracted from the loess should agree with those extracted from the lava, at least to within reasonable error estimates. Post-depositional chemical alteration is responsible for much of the source of errors in intensity estimates (Merrill and McElhinny, 1983), therefore, this comparison is attractive since loess and lava have very different chemical composition. The difference in intensity between the loess and lava is about 8 μT. On the other hand, the directions differ by only about 2°. The Chinese lava data from Tongjing has only a single transitional direction, corresponding to a VGP in the middle of Africa.

● We accept directional and absolute intensity data from Tongjing in this compilation, obtained from Table 1 of Zhu et al. (1991).

B.1.6. Hawaii

Baksi et al. (1992) analyzed samples from Haleakala Volcano in the Hawaiian island of Maui. In this reconnaissance study, two to three oriented samples per lava flow were collected (Hsu, personal communication) spanning the duration of the Matuyama–Brunhes RTF. Samples from all flows

were step-wise AF demagnetized up to 50–60 mT (Hsu, personal communication), and less than 25 mT was sufficient to remove overprint. Intensity is reported as unnormalized NRM [Intensity]. Four consecutive transitional directions were measured. α_{95} is not reported. Flows were dated by the Ar–Ar method: flow 3, which corresponds stratigraphically to the oldest flow was dated at > 0.850 Ma, indicating that it records an excursion well before the Matuyama–Brunhes transition; the three younger flows 4–6 have an average age of 0.783 Ma. Thus, the Hawaii data represents a partial recording of the Matuyama–Brunhes RTF.

B.1.7. Discussion of Hawaii

The Hawaiian data show no pattern in only a very few transitional field directions.

● We accept directional data from Hawaii in this compilation, obtained from Table 1 of Baksi et al. (1992).

● We do not accept intensity data from Hawaii in this compilation.

B.1.8. Chile

Brown et al. (1994) analyzed samples from Volcan Tatara-San Pedro in the central Chilean Andes. Oriented samples were step-wise AF demagnetized up to 80 mT. Mineralogical analysis was conducted (Pickens, personal communication), but this has not yet been published and intensity is reported as unnormalized NRM [Intensity]. Ten transitional directions were measured. No α_{95} exceeds 30°. Flows were dated by the K–Ar and Ar–Ar method, and all the transitional flows were unambiguously determined to belong to the Matuyama–Brunhes transition.

B.1.9. Discussion of Chile

We note that the single normal direction reported is dated at 0.33 Ma. The Chilean lava data exhibit a single abrupt change in declination followed by an abrupt change in inclination, with transitional VGPs which cluster around Australia like the VGP clusters found by Hoffman (1992) from Hawaiian data covering other reversals.

● We accept directional data from Chile in this compilation, obtained from Table 1 of Brown et al. (1994).

● We do not accept intensity data from Chile in this compilation.

B.1.10. Canary Islands

Quidelleur and Valet (1996) analyzed samples from La Palma, Canary Islands. Two adjacent sequences were sampled, one from the Barranco de Las Lomadas (LL) and the other from Los Sauces (LS). Samples were oriented by sun compass or magnetic compass; Quidelleur and Valet preferred solar azimuths, and applied a 5° W correction to the magnetic azimuths. Three to fifteen samples per lava flow were collected, spanning the duration of the Matuyama–Brunhes RTF. For each flow, samples were step-wise AF demagnetized up to 100 mT, and duplicate samples were step-wise T demagnetized up to 590°C; generally, 10 mT and 350°C was sufficient to remove overprint. ARM, IRM and χ were measured for each flow, and found to vary by a factor of ~ 5, indicating significant variation in the concentration of the magnetic carrier from one flow to another. ARM/χ also showed considerable variation, up to a factor of ~ 5, indicating considerable variation in the magnetic grain size; the magnetic carrier was judged to be magnetite to titanomagnetite. Absolute intensity was estimated by Thellier method, with corrections for mineralogical variations. No transitional directions were measured from either sequence [Resolution]. The LL sequence records an excursion sometime after the transition, but the date of these flows has, unfortunately, not been determined and it may not be part of the Matuyama–Brunhes transition [Date]. None of the LS samples have been dated [Date]. No α_{95} exceeds 30°.

● We do not accept data from Canary Islands in this compilation.

B.2. Lake sediments

B.2.1. Lake Tecopa

B.2.1.1. Tecopa 1. Hillhouse and Cox (1976) first studied samples from the Lake Tecopa site, east of Death Valley, CA. Three to six oriented samples were taken at each stratigraphic level. Pilot samples were step-wise AF demagnetized up to 20 mT, and a blanket demagnetization of 15 mT was applied to the remaining samples. Intensity was estimated by un-

normalized NRM after partial AF demagnetization at 15 mT [Intensity]. ARM was found to vary by a factor of ~ 2 over the depth of the transition; the magnetic carrier is not reported, but was later found by Valet et al. (1988) to be magnetite. Multiple transitional directions were measured. One direction has α_{95} which exceeds 30° [Scatter].

B.2.1.2. Tecopa 2. Valet et al. (1988) resampled the Tecopa site. Two to three oriented samples were taken at each stratigraphic level. Samples were step-wise AF demagnetization up to 50 mT and identical samples were step-wise T demagnetized to over 600°C. Relative intensity was estimated by NRM/ARM after partial T demagnetization at 300°C. ARM, SIRM and χ were found to vary by a factor of ~ 2 over the depth of the transition; SIRM, ARM and thermomagnetic analyses indicated that the primary magnetic carrier is magnetite. Multiple transitional directions were measured. α_{95} is not reported.

B.2.1.3. Tecopa 3. Larson and Patterson (1993) analyzed samples from the same locality studied by Hillhouse and Cox and Valet et al., plus samples from an additional locality. Oriented samples were subjected to a preliminary AF demagnetization at 15 mT, then the samples were step-wise T demagnetized up to 610°C. Intensity was estimated by unnormalized NRM after partial AF and T demagnetization at 15 mT and 610°C [Intensity]. No analysis of the magnetic mineralogy with depth is reported [Mineral]; thermomagnetic analysis indicated that the primary magnetic carrier is magnetite with an abundance of titanomagnetite and hematite. A few intermediate directions were measured. α_{95} is not reported.

B.2.1.4. Discussion of Tecopa. Valet et al. could not reproduce the directions obtained by Hillhouse and Cox after AF demagnetization, and furthermore, T demagnetization yielded directions which were inconsistent with both their own AF results and those of Hillhouse and Cox [Demag.]. This problem was severe enough that some samples yielded normal magnetization after AF cleaning, but identical samples yielded reverse magnetization after T cleaning, see Figure 6 of Valet et al. (1988). Both studies found transitional VGPs confined to longitudinal bands, but those of Hillhouse and Cox are 120° east of those of Valet et al., compare Figure 7 of Hillhouse and Cox (1976) with Figure 8 of Valet et al. (1988). Larson and Patterson found yet more mutually contradictory records of the RTF [Consistency]. Larson and Patterson concluded that the sediments from Lake Tecopa are contaminated by post-depositional remanent magnetization (PDRM) and chemical remanent magnetization (CRM) [Author Judge].

● We do not accept any Lake Tecopa data in this compilation.

B.2.2. Bishop

Liddicoat (1993) analyzed samples from three separate localities near Owens Lake, Bishop, CA. Samples were oriented; Liddicoat reports an orientation accuracy of $\pm 2°$. Three to six samples were taken at each stratigraphic level. Pilot samples from each stratigraphic level were subjected to step-wise AF demagnetization up to 80 mT, finding that 20 mT removed most of the overprint. Most of the remaining samples were blanket AF demagnetized at 20 mT. A few samples were step-wise T demagnetized up to 625°C. Intensity was estimated by unnormalized NRM after partial AF demagnetization at 20 mT [Intensity]. No analysis of the magnetic mineralogy with depth is reported [Mineral]; thermomagnetic magnetic analysis indicated that the primary magnetic carrier is magnetite with some hematite. Locality A1 gave only one transitional direction [Resolution], A2 gave only two consecutive transitional directions, A3 gave three transitional directions but only two are consecutive [Resolution]. The data exhibit a great deal of scatter: α_{95} exceeds 30° for all transitional data at all three sites [Scatter] (see Table 1 of Liddicoat, 1993). Liddicoat concludes that the data do not capture the true behavior of the paleomagnetic field [Author Judge].

● We do not accept any Bishop data in this compilation.

B.3. Loess

B.3.1. European sites

B.3.1.1. Červený Kopec 1. Bucha (1970) analyzed samples from Červený Kopec (Red Hill) near Brno

Czechoslovakia. Oriented samples were collected at 2-cm intervals from a stratigraphic layer 4 m thick. After experimenting with AF and T demagnetization and simple reorientation of the samples in the earth's ambient magnetic field, Bucha concluded that overprint could be removed by simply reorienting the samples so that their magnetic vectors were directed opposite the earth's and then waiting a week [Demag.] (see p. 258 of Bucha, 1970). Absolute intensity was estimated from laboratory resedimentation experiments of slurries made from field samples [Intensity]. No analysis of the magnetic mineralogy is reported [Mineral]; some change in the color of the sediments is noted. Several transitional directions were measured. The author was unable to determine if the transitional data belong to the Matuyama–Brunhes transition or the Lower Jaramillo [Date] (see p. 260 of Bucha, 1970). α_{95} is not reported.

B.3.1.2. Červený Kopec 2, Suchdol. Kočí et al. (1974) analyzed samples from Červený Kopec and from Suchdol near Prague. The orientation of the samples is not reported. A blanket AF demagnetization of 20 mT was applied to the samples, but no step-wise demagnetization of any samples is reported [Demag.]. Some analysis of the magnetic mineralogy was performed, but its variation with depth is reported [Mineral]; the magnetic carrier is not reported. Intensity for Červený Kopec 2 is not reported [Intensity]; intensity for Suchdol was estimated by unnormalized NRM after partial AF demagnetization at 20 mT [Intensity]. We note that the Matuyama–Brunhes RTF at the Suchdol site occurs over a boundary between two different types of soils (see Figure 1 of Kočí et al., 1974) which may indicate a temporal interruption of the record. α_{95} is not reported.

B.3.1.3. Brüggen, Regensburg, Krems. Kočí and Šibrava (1976) analyzed samples from Brüggen north-west Germany, Regensburg southern Germany, and Krems north-east Austria. The orientation of the samples is not reported. No demagnetization is reported [Demag.]. Intensity is not reported [Intensity], nor is any analysis of magnetic mineralogy reported [Mineral]. A resampling of the Brüggen site failed to find a convincing record of the Matuyama–Brunhes RTF (Laj, personal communication), thus, the data from this site appear to be irreproducible. Kočí and Šibrava characterize the data from Regensburg as approximate and note that orientation of the site may have shifted due to tectonic movement (see p. 141 of Kočí and Šibrava, 1976). We note that the Matuyama–Brunhes RTF at Regensburg occurs over different stratigraphic layers, which may indicate a temporal interruption of the record. α_{95} is not reported.

● We do not accept any European loess data in this compilation.

B.3.2. Chinese sites

B.3.2.1. Xifeng 1. Sun et al. (1993) investigated the western edge of the Xifeng loess plateau in north-central China, south of the Great Wall. The environment has a high sedimentation rate ($\sim$ 10 cm/kyr). Single oriented samples were taken every 2.4 cm from a 3.8-m section of the L8 loess. Each sample was step-wise T demagnetized up to 700°C. Intensity was estimated by unnormalized NRM after partial T demagnetization at 350°C [Intensity]. The authors conclude that there is little change in the grain size across the transitional depth, but they note some change in sediment color and a variation in χ by a factor of ~ 4 over the stratigraphic height of the transition [Mineral]. Nonetheless, Sun et al. argue that the magnetic carrier is relatively constant. Thermomagnetic analysis indicated that the primary magnetic carrier is magnetite; some magnetite was also found. Multiple transitional directions were measured. α_{95} is not reported.

B.3.2.2. Xifeng 2. Zhu et al. (1993) also investigated the eastern edge of the Xifeng loess plateau. Oriented samples in eight vertically parallel groups from a 2.7-m section of the L8 loess were taken every 2–2.5 cm. Each sample was step-wise T demagnetized up to 710°C. Relative intensity was estimated by NRM/ARM after partial T demagnetization at 300°C. Zhu et al. report only $\sim$ 10% variation in χ from five samples spanning the stratigraphic height of the transition, a result which should be contrasted with that of Xifeng 1. IRM analysis and thermomagnetic analysis indicated that the primary magnetic carrier is magnetite. Only one transitional direction

was measured [Resolution]. α_{95} is less than about 15° for most of the directions, no α_{95} exceeds 30°.

B.3.2.3. Weinan. Zhu et al. (1994) analyzed samples from Weinan, ~ 200 km south-east of Xifeng. The environment has a high sedimentation rate (~ 9.3 cm/kyr). Samples were oriented by both magnetic and sun compasses. Samples in two vertically parallel groups from a 1.8-m section of the L8 loess were taken every 0.5–1.0 cm, each was step-wise T demagnetized up to 700°C. Intensity was estimated by unnormalized NRM after partial T demagnetization at 380°C. Hysteretic analysis indicated that the magnetic grain size does not change much across the transitional section. Zhu et al. report only ~ 10% variation in χ from a sparse two samples within the stratigraphic height of the transition. IRM, thermomagnetic analyses and X-ray diffraction spectra showed that the primary magnetic carrier is magnetite with some hematite. Eleven transitional directions were measured. α_{95} is not reported.

B.3.2.4. Discussion of Chinese loess. Despite the apparent completeness of the two Xifeng studies, the records of the RTF are significantly different and are obviously inconsistent. The directional transition of Xifeng 1 lasted for ~ 14 800 years, exhibiting multiple changes of polarity, while for Xifeng 2, the directional transition lasted for ~ 3600 years, exhibiting only a few abrupt changes of polarity. Zhu et al. suggested that these differences may be due to different levels of pedogenesis. On the other hand, with a minor linear adjustment of the depth scale, the Xifeng 2 data correlate extremely well with the Weinan data, while the data of Xifeng 1 is inconsistent with the Weinan and Xifeng 2 data [Consistency]; compare Figure 3 of Sun et al. (1993) with Figure 6 of Zhu et al. (1993). The Weinan loess data exhibit several fluctuations in inclination and declination; transitional VGPs are concentrated along Asian–Australian longitudes and the directional transition took ~ 5000 years.

● We do not accept any Xifeng loess data in this compilation.

● We accept directional and relative intensity data from Weinan in this compilation, measured by Zhu et al. at the Centre des Faibles Radioactivités.

B.4. Shallow-marine sediments

B.4.1. Boso, Japan

B.4.1.1. Yanagawa. Niitsuma (1971) analyzed samples from the sediments deposited in the shallow-marine environment now situated on the Boso Peninsula of central Japan. These siltstone sediments were deposited very rapidly (~ 370 cm/kyr), but Niitsuma concluded that they accumulated under calm conditions. Samples were oriented. Samples were taken every 1 m over a 40-m section of sediment. Once the transitional period was identified, additional samples were taken every 10 cm over a 4-m section spanning the duration of the Matuyama–Brunhes RTF. Samples from Yanagawa were AF demagnetized up to 9 mT; it is not indicated if this was step-wise [Demag.]. Relative intensity was estimated by NRM/IRM after partial AF demagnetized at 9 mT. No details of the variation of the magnetic mineralogy with depth is reported [Mineral]. Multiple transitional directions were measured. The data appear to be very noisy; multiple transitional directions have standard errors in inclination of more than 10° and in declination of more than 30° [Scatter].

B.4.1.2. Heizogawa. Okada and Niitsuma (1989) analyzed samples from the Heizogawa and Chonan sections of the Boso Peninsula, respectively 8.5 and 14 km from Yanagawa. Samples were oriented. Samples were taken about every 2–3 cm over a section spanning the duration of the Matuyama–Brunhes RTF. Pilot samples were AF step-wise demagnetized up to 30 mT, and a blanket demagnetization of 15–20 mT was applied to the remaining samples. Relative intensity was estimated by NRM/ARM after partial AF demagnetization at 30–40 mT, but was only estimated for a very few points. ARM varies by a factor of ~ 2 over the depth of the transition; no mention is made of the magnetic carrier. Multiple transitional directions were measured. Numerous directions have α_{95} exceeding 30° [Scatter].

B.4.1.3. Discussion of Boso. Of the three Boso data sets, the Yanagawa data have the most dispersion during the polarity transition (see Figure 6 of Okada

and Niitsuma, 1989). There is some broad consistency between the Heizogawa and Chonan data sets. Finally, we note that the two polarity transitions recorded in this data could correspond to the multiple polarity transitions found, for example, in the Weinan Chinese loess data. If this is true then the Boso data might be only a partial recording of the overall Matuyama–Brunhes RTF; note that for the estimated sedimentation rates, the Heizogawa and Chonan data sets represent only ~ 1200 years of time.

● We do not accept Boso Yanagawa data in this compilation.

● We accept directional Boso Heizogawa and Chonan data in this compilation, which we obtained by scanning Figure 6 of Okada and Niitsuma (1989), then computing the mean directions and α_{95}. We have not scanned the few relative intensity measurements.

B.4.2. Wanganui, New Zealand

Turner and Kamp (1990) analyzed samples from the Castlecliff site of the Wanganui Basin of the North Island, New Zealand. An estimate of the sedimentation rate is not reported, but Roberts and Pillans (1993) estimate it to be in the 10's of cm/kyr. Four oriented samples per stratigraphic level were collected at nonuniformly distributed stratigraphic heights. The Matuyama–Brunhes RTF is recorded in the Kaikokopu Shell Grit and Upper Westmere Siltstone. Samples were step-wise T demagnetized up to 375°C; Turner and Kamp found that higher temperatures induced changes in the magnetic mineralogy. Intensity is not reported [Intensity]. ARM, SIRM and χ were measured for several samples determined to span the Matuyama–Brunhes transition. SIRM/χ and SIRM/ARM from two samples from the Upper Westmere Siltstone differ by ~ 10%, with variations of a factor of ~ 3 over the different stratigraphic units, thus, indicating good uniformity of the magnetic grain size despite evident differences in sediment composition. Five transitional directions were measured. One of the transitional directions was measured in the Kaikokopu Shell Grit, with the remaining measured in the Upper Westmere Siltstone; this may indicate a temporal interruption of the record. α_{95} is not reported.

B.4.2.1. Discussion of Wanganui. Roberts and Pillans (1993) measured SIRM/χ from the neighboring Whanagaehu site, ~ 30 km from Wanganui, and found significant differences between the Upper Westmere Siltstone and other stratigraphic units; SIRM/χ differs by a factor of ~ 5. Turner and Kamp conclude that the magnetic carrier is primarily magnetite, although they suggest that there may have been some post-depositional chemical changes; Roberts and Pillans suggest that greigite or pyrrhotite may be present in the Upper Westmere Siltstone. We note that Pillans et al. (1994) do not report any Matuyama–Brunhes transitional directions in their analysis of the Wanganui Basin, although because of the sparsity of sampling, this is not necessarily a sign of inconsistency. Note that a few of the VGPs shown in Figure 7 of Turner and Kamp (1990) were incorrectly plotted (Turner, personal communication).

● We accept directional data from Wanganui in this compilation, obtained from Turner (personal communication).

B.5. Deep-ocean sediments

B.5.1. Pacific Ocean sites

B.5.1.1. Papagayo. Harrison and Somayajulu (1966) analyzed samples from north-western Pacific core Papagayo 3G. This core was azimuthally oriented. The core was taken from a low sedimentation rate environment (~ 0.2 cm/kyr) [Sed. Rate]. Samples were taken every 5 cm along core length, spanning the duration of the Matuyama–Brunhes RTF; additional measurements over the depth of the transition were made by sampling every 0.5 cm. All samples were step-wise AF demagnetized up to 12 mT. Intensity was estimated by NRM/χ after partial AF demagnetization at 10 mT. Some analysis of the variation of magnetic mineralogy is reported, the magnetic carrier is not reported. Few transitional directions were measured.

● We do not accept Papagayo data in this compilation.

B.5.1.2. KH70-2-5. Kawai et al. (1973) analyzed samples from Pacific core KH70-2-5. No mention is made of the azimuthal orientation of the core. The

core was taken from a low sedimentation rate environment (~ 0.1 cm/kyr) [Sed. Rate]. Horizontal slices were taken every 2 mm along core length, spanning the duration of the Matuyama–Brunhes RTF. Relative intensity was estimated by NRM/SIRM; the partial demagnetization strength is not reported. No details of the analysis of the magnetic mineralogy with depth is reported [Mineral]; the magnetic carrier is not reported. A few transitional directions were measured.

● We do not accept data from KH70-2-5 in this compilation.

B.5.1.3. KH73-4-7, KH73-4-8. Kawai et al. (1975, 1977) analyzed samples from Pacific cores KH73-4-7 and KH73-4-8. No mention is made of the azimuthal orientation of the cores. These cores were taken from low sedimentation rate environments (~ 0.6 cm/kyr) [Sed. Rate]. Horizontal slices were taken every 0.4 cm along core length, spanning the duration of the Matuyama–Brunhes RTF. Pilot samples were step-wise AF demagnetized up to 50 mT, and a blanket demagnetization of 10 mT was applied to the remaining samples. Relative intensity was estimated by NRM/SIRM after partial AF demagnetization at 10 mT. SIRM varies by a factor of ~ 2 over the sampled depth; the magnetic carrier is not reported. Several transitional directions were measured.

● We do not accept data from KH73-4-7 in this compilation.

B.5.1.4. RC10-167. Kent and Opdyke (1977) analyzed samples from north-western Pacific core RC10-167. No mention is made of the azimuthal orientation of the core. Declination is not reported [*I* and *D*]. This core was taken from a low sedimentation rate environment (~ 2.1 cm/kyr) [Sed. Rate]. Samples were taken every 3.3 cm along core length, spanning the duration of the Matuyama–Brunhes RTF. Pilot samples were step-wise AF demagnetized up to 40 mT, and a blanket demagnetization of 15 mT was applied to the remaining samples. Relative intensity was estimated by NRM/ARM after partial AF demagnetization at 15 mT. ARM varies by a factor of ~ 3 over the sampled depth; the magnetic carrier is not reported. One or two transitional directions were measured [Resolution].

● We do not accept data from RC10-167 in this compilation.

B.5.1.5. RC9-114, RC9-119, RC10-182, RCI5-21, V20-104, V20-107, V20-108. Clement et al. (1982) and Clement and Kent (1984) analyzed samples from several Pacific cores, mostly distributed along the 180° meridian. These azimuthally unoriented cores were rotated so that directions before and after the transition are in agreement with an axial dipole. Unfortunately, all of these cores come from low sedimentation rate environments (less than ~ 1.2 cm/kyr) [Sed. Rate]. Samples were taken every 4–5 mm along core length, spanning the duration of the Matuyama–Brunhes RTF. Pilot samples of all of these cores were step-wise demagnetized up to 60 mT, and a blanket demagnetization of 10–20 mT was applied to the remaining samples. Intensity was estimated by unnormalized NRM, after partial AF demagnetization at 10–20 mT [Intensity]. ARM measurements on pilot samples indicated that the primary magnetic carrier is magnetite or titanomagnetite (Clement, personal communication), but no analysis of mineralogy with depth is reported [Mineral]. With the exception of RC9-119 [Resolution], all of these cores record three or more consecutive transitional directions. Clement et al. have remarked that some of these cores are not especially consistent (see Figure 2 of Clement et al., 1982) [Consistency]; they speculate that this may be due to varying lock-in depths caused by magnetic grains of different size.

● We do not accept data from RC9-114, RC9-119, RC10-182, RC15-21, V20-104, V20-107 and V20-108 in this compilation.

B.5.1.6. K78-10-19, K78-10-30. Theyer et al. (1985) analyzed samples from equatorial Pacific cores K78-10-19 and K78-10-30. These azimuthally unoriented cores were rotated so that directions before and after the transition are in agreement with an axial dipole. K78-10-19 was taken from a low sedimentation rate environment (~ 1.7 cm/kyr) [Sed. Rate], while K78-10-30 was taken from a high sedimentation rate environment (~ 3.5 cm/kyr). Samples were taken every ~ 0.5 cm along core length, spanning the duration of the Matuyama–Brunhes RTF. Pilot sam-

ples were step-wise AF demagnetized up to 60 mT, and a blanket demagnetization of 10–12.5 mT was applied to the remaining samples. Relative intensity was estimated by NRM/ARM after partial AF demagnetization at 12.5 mT. ARM intensity is fairly constant, varying by less than a factor of ~ 2 over the depth of the transition, indicating good uniformity in concentration of the magnetic carrier with depth. ARM analysis indicated that the primary magnetic carrier is magnetite. Minor changes in sediment color with depth were noticed. Multiple intermediate directions were measured, but in neither core were three consecutive transitional directions measured [Resolution]. Data from both of these cores appear to have a very high noise content.

● We do not accept data from K78-10-19 and K78-10-30 in this compilation.

B.5.1.7. 767B, 769A. Schneider et al. (1992) and Kent and Schneider (1995) analyzed samples from western-equatorial Pacific cores 767B and 769A. These cores were azimuthally unoriented. Both of these cores were taken from high sedimentation rate environments (~ 8–11 cm/kyr). For 767B, no discrete samples were demagnetized [Demag.], measurements with a shipboard pass-through magnetometer were taken every 10 cm along the length of the core. Other paleomagnetic groups took discrete samples from the transitional section of 767B, but results have not yet been published (Hsu, personal communication). For 769A, discrete samples taken about every 10 cm were step-wise AF demagnetized, the maximum field strength is not reported, but most of the overprint was removed after partial demagnetization at 20 mT. No directions are reported in the paper [I and D], only VGP latitude is reported. Intensity was estimated by NRM/ARM and NRM/χ after partial AF demagnetization at 10 mT for 767B and 20 mT for 769A; the magnetic carrier is not reported. One transitional direction was measured in 767B, and two consecutive transitional directions were measured from 769A [Resolution]. The main emphasis of Schneider et al. (1992) is the temporal order of the Matuyama–Brunhes transition and a cataclysmic meteorite impact, but they find these two events to be acausal.

● We do not accept data from 767B and 769A in this compilation.

B.5.1.8. 792A. Cisowski and Koyama (1992) analyzed samples from northern Pacific core 792A. The core was azimuthally oriented. This core was collected from a very high sedimentation rate environment (~ 8.1 cm/kyr). Samples were taken at irregular depth intervals. Most samples were step-wise AF demagnetized up to 100 mT, and some samples were AF-continuous-T demagnetized. Relative intensity was estimated by NRM/ARM after AF demagnetization at 100 mT. ARM and χ vary by a factor of ~ 20, indicating significant variation in the concentration of magnetic carrier over the depth of the transition [Mineral], but ARM/χ indicates good uniformity of magnetic grain size. ARM and IRM analyses indicated that the primary magnetic carrier is magnetite. Some variation of sediment color with depth is reported. Only one transitional direction was measured [Resolution]. The authors note some inconsistency between the intensity data prior to the directional transition from core 792A and neighboring, but incompletely recovered, core 791B. They speculate that the sediments of 792A may have been disrupted.

● We do not accept data from 792A in this compilation.

B.5.1.9. 851D. Valet and Meynadier (1993) analyzed samples from eastern-equatorial Pacific core 851D. No mention is made of the azimuthal orientation of the core. The core was taken from a low sedimentation rate environment (~ 2.0 cm/kyr) [Sed. Rate]. Measurements with a shipboard pass-through magnetometer were taken every 2 cm along the length of the core. Discrete samples were step-wise AF demagnetized, the maximum field strength is not reported. ARM, IRM and χ were measured, the ratio ARM/χ indicates good uniformity of grain size with depth. The magnetic carrier is not reported. No declinations are reported [I and D]. Relative intensity was estimated by NRM/ARM, NRM/IRM and NRM/χ.

B.5.1.10. Discussion of 851D. The main emphasis of Valet and Meynadier (1993) is interreversal intensity variations. 851D shows a sawtooth variation with time, a rapid increase in intensity after a reversal followed by a slow but varying decrease in intensity leading up to another reversal. This phenomenon

may be an artifact of overprinting (Mazaud, 1996; Kok and Tauxe, 1996), although this idea has been contested (Meynadier and Valet, 1996).

● We do not accept data from 851D in this compilation.

B.5.1.11. 803B, 804C, 805B. Hartl and Tauxe (1996) analyzed samples from western-equatorial Pacific cores 803B, 804C and 805B. These azimuthally unoriented cores were rotated so that directions before and after the transition are in agreement with an axial dipole. These cores were collected from low sedimentation rate environments (~ 1–2 cm/kyr) [Sed. Rate]. Samples were taken every 1–3 cm along core length, spanning the duration of the Matuyama–Brunhes RTF. All samples were step-wise AF demagnetized up to 85 mT, and selected duplicate samples were step-wise T demagnetized up to 600°C. Relative intensity was estimated by NRM/ARM, NRM/IRM and NRM/χ after partial AF demagnetization at 20 mT. The ratios ARM/χ and IRM/χ indicated good uniformity of magnetic grain size. Few transitional directions were measured. The main emphasis of Hartl and Tauxe (1996) is intensity variations prior to the Matuyama–Brunhes transition.

● We do not accept data from 803B, 804C and 805B in this compilation.

B.5.2. Atlantic Ocean sites

B.5.2.1. V30-45. Clement and Kent (1984) analyzed samples from equatorial Atlantic core V30-45. This azimuthally unoriented core was rotated so that directions before and after the transition are in agreement with an axial dipole. This core comes from a low sedimentation rate environment (less than ~ 0.5 cm/kyr) [Sed. Rate]. Samples were taken every 4–5 mm along core length, spanning the duration of the Matuyama–Brunhes RTF. Pilot samples were step-wise demagnetized up to 60 mT, and a blanket demagnetization of 10–20 mT was applied to the remaining samples. Intensity was estimated by unnormalized NRM, after partial AF demagnetization at 10–20 mT [Intensity]. No analysis of the magnetic mineralogy with depth is reported [Mineral]. ARM measurements indicated that the primary magnetic carrier is magnetite or titanomagnetite (Clement, personal communication). No transitional directions were measured [Resolution].

● We do not accept data from V30-45 in this compilation.

B.5.2.2. 606A, 607A, 609B, 610B, 610C. Clement and Kent (1986) analyzed samples from five north Atlantic cores, 606A, 607A, 609B, 610B and 610C. These azimuthally unoriented cores were rotated so that directions before and after the transition are in agreement with an axial dipole. The cores were taken from high sedimentation rate environments (greater than ~ 3 cm/kyr in all cases). Samples were taken every 0.5 cm along each core length, spanning the duration of the Matuyama–Brunhes RTF. Pilot samples were step-wise AF demagnetized up to 80 mT, and a blanket 10–30 mT was applied to the remaining samples. Demagnetization did not successfully isolate the characteristic field directions in 606A and 607A [Demag.]. ARM analysis for 609B was conducted over the depth of the Matuyama–Brunhes RTF, but details are not reported for the remaining cores [Mineral]. 610C does not record the entire transition due to incomplete recovery of the core. The authors conclude that 606A, 610B and 610C are excessively noisy [Author Judge].

B.5.2.3. Discussion of 609B. Clement et al. conclude that 609B, which, among this group of cores, has the highest sedimentation rate (~ 5.9–8.3 cm/kyr), records faithfully the Matuyama–Brunhes RTF. Relative intensity was estimated by NRM/ARM after partial AF demagnetization at 20 mT. ARM varies by a factor of ~ 2 over the depth of the transition, indicating fairly good uniformity of the magnetic carrier, which was judged to be magnetite or titanomagnetite (Clement, personal communication). Five transitional directions were measured. The core was reasonably complete; the apparent post-reversal scatter in declination is due primarily to intermittent relatively steep inclinations; note the average VGP latitude for the 14 measurements made between depths −8.5 and −1.5 cm is 62.35°. Transitional VGPs are concentrated along American longitudes; the directional transition lasted for ~ 2300 years.

● We do not accept any data from 606A, 607A, 610B and 610C in this compilation.

● We accept directional and relative intensity data from 609B in this compilation, obtained from Athanassopoulos (personal communication).

B.5.2.4. 642B, 642C, 643A, 644A. Schönharting et al. (1989) analyzed samples from four extreme-north Atlantic cores, 642B, 642C, 643A and 644A. These cores were azimuthally unoriented; relative declinations were deemed unreliable [I and D]. 643A was taken from a low sedimentation rate environment ($\sim$ 2.0 cm/kyr) [Sed. Rate], while 642B, 642C and 644A were taken from high sedimentation rate environments ($\sim$ 4.0–10.0 cm/kyr). All samples were step-wise AF demagnetized up to 60 mT, usually 10–15 mT was sufficient to remove overprint, except for 644A for which overprinting could not be removed [Demag.]. Relative intensity was estimated by NRM/χ, NRM/ARM and NRM/SIRM, after partial AF demagnetization at 10 mT. Susceptibility varies by a factor of $\sim$ 2 over the sample depth; the magnetic carrier is not reported. One or two consecutive transitional directions were measured in 642B, 642C and 643A [Resolution]. Data from these three cores are roughly consistent.

● We do not accept data from 642B, 642C, 643A and 644A in this compilation.

B.5.2.5. 659C, 664D, 665B. Valet et al. (1989) analyzed samples from three equatorial Atlantic cores. 664D and 665B were located almost precisely on the equator, while 659C came from a moderate northern latitude. The cores were azimuthally unoriented and rotated so that directions before and after the transition are in agreement with an axial dipole. 665B was taken from a low sedimentation rate environment, ($\sim$ 1.5 cm/kyr) [Sed. Rate]; 659C and 664D were taken from high sedimentation rate environments (greater than 3 cm/kyr). Samples were taken every 0.5–1.0 cm along core length, spanning the duration of the Matuyama–Brunhes RTF. All samples were step-wise AF demagnetized up to 60 mT, or step-wise T demagnetized. Overprint was removed from 659C with 5 mT, 664D and 665B with 15 mT. Relative intensity was measured by NRM/ARM after partial AF demagnetization at 20 mT. ARM and χ vary by a factor of $\sim$ 2 over the depth of the transition; thermomagnetic analyses and IRM analysis indicated that the primary magnetic carrier is magnetite. There was no indication of variation in sediment color. No more than two consecutive transitional directions were measured from 659C, none were measured from 665B [Resolution], but nine transitional directions were measured from 664D. 659C has several transitional inclinations, but almost no transitional declinations. The discrepancy between the data from 664D and 665B is curious since they came from neighboring sites; the authors speculate that the lack of transitional directions from 665B was due to overprinting during directional lock-in of magnetic particles, a problem they attribute to a low sedimentation rate (see p. 376 of Valet et al., 1989).

B.5.2.6. Discussion of 664D. The 664D data exhibit a smooth variation in declination, together with relatively smaller fluctuations in inclination about zero; since 664D was located almost exactly on the equator, such directional changes indicate that the Matuyama–Brunhes RTF is not axisymmetric (Valet et al., 1989). The transitional VGPs of 664D are concentrated along western Asian longitudes and the directional transition took $\sim$ 3900 years.

● We do not accept any data from 659C and 665B in this compilation.

● We accept directional and relative intensity data from 664D in this compilation, obtained from Valet (personal communication).

B.5.3. Indian Ocean site

B.5.3.1. V16-58. Clement and Kent (1991) analyzed samples from southern hemisphere core V16-58. This core was azimuthally unoriented; the core was rotated so that directions before and after the transition are in agreement with an axial dipole. The core was taken from a reasonably high sedimentation rate environment ($\sim$ 4.0 cm/kyr). Kent and Schneider (1995) discuss uncertainties in the sedimentation rate of the V16-58 site. Samples were taken every 0.5 cm along core length, spanning the duration of the Matuyama–Brunhes RTF. Each slice was split into two or three parts for redundant measurement. All samples were step-wise AF demagnetized up to 50 mT. Relative intensity was estimated by NRM/ARM after partial AF demagnetization at 20 mT. ARM varies by $\sim$ 10% over the depth of the transition indicating good uniformity of the magnetic carrier,

which was judged to be magnetite or titanomagnetite (Clement, personal communication). Six transitional directions were measured; the directional transition lasted for ~ 4700 years.

B.5.3.2. Discussion of V16-58. The data of V16-58 exhibit multiple fluctuations in declination superimposed on a smooth variation and an abrupt change in inclination, followed by fluctuations. Transitional VGPs are concentrated along American longitudes and the directional transition took ~ 4700 years.

● We accept directional and relative intensity data from V16-58 in this compilation, obtained from Athanassopoulos (personal communication).

Appendix C. Data

The data of MBD97 are listed in Tables 3–8 in temporal order (stratigraphic order), starting with the oldest values (lowest stratigraphic level).

Table 3
Data of MBD97

Flow	#	Dec.	Inc.	Ab. int. (μT)	α_{95}	Lat. (° N)	Long. (° E)	Pol.	Age (Ma)
Tahiti, Punaruu, −17.7° N, 210.3° E									
R1A	4	−191.6	40.9	–	2.9	−77.7	270.6	R	–
R1B	5	−187.8	34.8	–	3.1	−82.5	287.9	R	–
R1C	5	−174.2	37.8	–	2.6	−83.5	153.8	R	–
R1D	5	−217.0	15.6	–	5.5	−52.7	310.6	I	–
R1E	4	−168.7	24.7	–	11.4	−78.1	98.3	R	–
R1F	6	−166.8	26.7	–	3.7	−76.8	106.4	R	–
R1G	7	−168.4	21.6	–	5.6	−77.0	91.8	R	–
R1H	6	−181.0	11.0	–	3.7	−77.8	25.6	R	–
R1I	6	−183.1	14.2	–	3.5	−79.1	13.8	R	–
R1J	6	−185.1	39.4	–	1.5	−83.3	255.4	R	–
R1K	9	−180.2	36.6	–	2.9	−87.3	214.3	R	–
R1L	5	−184.8	36.5	–	2.5	−84.8	269.7	R	–
R1M	5	−183.8	36.7	–	2.8	−85.5	262.4	R	–
R1N	6	−181.8	33.3	37.7	3.3	−88.2	284.3	R	–
R1O	6	−182.9	39.7	–	2.5	−84.4	239.2	R	–
R1P	6	−178.9	44.9	–	2.8	−81.2	203.9	R	–
R1Q	5	−177.4	50.6	–	4.1	−76.2	201.0	R	–
R1R	6	−174.7	44.8	–	4.4	−80.0	181.8	R	–
R1S	6	−183.3	53.4	–	6.7	−73.5	220.0	R	–
R1T	5	−133.4	5.4	–	4.7	−41.9	107.6	T	–
R1U	4	−135.5	7.3	3.4	3.5	−44.2	107.8	T	–
R1V	5	−125.0	0.1	–	12.0	−33.1	108.3	T	–
TR-TS	5	−129.8	0.2	3.6	2.4	−37.6	106.2	T	–
TT	6	−127.1	−5.5	–	2.2	−34.0	104.3	T	–
PL	6	2.0	−43.6	–	7.0	82.0	17.2	N	–
TU	5	−1.4	−50.6	–	7.1	76.3	35.4	N	–
China, Tongjing, 37.8° N, 120.8° E									
LB	7	187.2	−54.3	51.6	6.4	−83.5	55.7	R	0.840
SB	12	185.1	−56.2	60.0	5.6	−85.8	43.7	R	–
US	7	−75.5	−10.4	17.9	6.3	8.1	17.7	T	–
UD	10	17.6	58.7	74.5	5.8	76.1	198.6	N	–
DD	20	−22.3	56.7	22.5	4.9	72.4	36.0	N	–
Hawaii, Haleakala, 20.7° N, 203.7° E									
1	?	190.9	−26.6	–	?	−77.6	144.7	R	–
2	?	189.1	−34.4	–	?	−81.2	124.3	R	–
3	?	90.9	−32.0	–	?	−6.9	309.7	T	0.850

Table 3 (continued)

Flow	#	Dec.	Inc.	Ab. int. (μT)	α_{95}	Lat. (° N)	Long. (° E)	Pol.	Age (Ma)
Tahiti, Punaruu, −17.7° N, 210.3° E									
4	?	137.4	−43.2	–	?	−50.7	308.5	T	0.772
5	?	−44.4	85.0	–	?	27.6	195.9	T	0.780
6	?	187.2	31.5	–	?	−51.6	192.6	T	0.787
7	?	−28.2	39.4	–	?	63.8	122.4	N	–
8	?	0.5	32.9	–	?	87.2	14.1	N	–
9	?	10.5	20.1	–	?	75.5	337.9	N	–
Chile, Tatara, −36.0° N, 289.0° E									
1	?	−173.9	40.7	–	6.3	−76.2	133.2	R	0.975
2	?	−149.8	−42.3	–	18.0	−23.1	138.9	T	0.704
3	?	−146.5	−63.9	–	19.3	−3.0	131.8	T	0.768
4	?	−124.7	−48.3	–	11.1	−6.5	155.2	T	–
5	?	−152.8	−50.8	–	12.5	−17.8	133.2	T	–
6	?	−151.5	−49.3	–	17.4	−18.6	134.8	T	–
7	?	−176.9	−59.0	–	19.0	−14.2	111.5	T	–
8	?	−159.6	−38.9	–	9.9	−28.9	130.7	T	–
9	?	−142.3	−42.5	–	12.7	−19.7	145.2	T	–
Chile, Tatara, −36.0° N, 289.0° E									
10	?	−173.4	−61.0	–	11.9	−11.7	114.0	T	–
11	?	−152.3	−47.2	–	10.8	−20.5	134.9	T	0.763
12	?	−5.5	−23.5	–	18.4	65.8	275.8	N	0.330

All angular measurements in degrees. # denotes the number of samples taken per stratigraphic level. The polarity states are denoted (R) reverse, (N) normal, (I) intermediate, (T) transitional.

Table 4
Data of MBD97

Height (cm)	#	Dec.	Inc.	Rel. int.	α_{95}	Lat. (° N)	Long. (° E)	Pol.
China, Weinan, 34.2° N, 109.2° E								
0.0	1	−154.0	−33.0	0.7225	–	−61.7	47.6	R
1.0	1	−159.0	−42.0	1.0000	–	−69.2	42.2	R
2.0	1	−165.0	−50.0	0.5331	–	−76.9	30.2	R
3.0	1	−161.0	−37.0	0.4966	–	−68.4	53.2	R
4.0	1	−167.0	−38.0	0.5463	–	−72.8	64.2	R
5.0	1	−161.0	−38.0	0.5419	–	−68.9	51.8	R
6.0	1	−177.0	−36.0	0.1689	–	−75.5	97.9	R
7.0	1	−170.0	−50.0	0.6193	–	−80.9	38.5	R
9.0	1	−197.0	−51.0	0.3311	–	−75.5	194.0	R
11.0	1	−177.0	−24.0	0.2741	–	−68.2	101.3	R
13.0	1	−149.0	−35.0	0.3354	–	−58.7	39.7	R
15.0	1	−171.0	−36.0	0.1290	–	−73.7	77.6	R
17.0	1	−175.0	−54.0	0.3720	–	−85.9	13.1	R
19.0	1	−185.0	−63.0	0.3199	–	−79.0	270.1	R
21.0	1	−174.0	−13.0	0.1699	–	−61.8	96.5	R
23.0	1	−167.0	−40.0	0.4323	–	−73.9	60.9	R
25.0	1	−174.0	−19.0	0.1436	–	−65.0	95.1	R
27.0	1	−180.0	−39.0	0.4104	–	−77.8	109.2	R
29.0	1	−167.0	−44.0	0.5204	–	−76.0	52.6	R
31.0	1	−171.0	−48.0	0.4737	–	−80.8	50.7	R
33.0	1	−187.0	−50.0	0.4109	–	−83.2	171.1	R
35.0	1	−156.0	−39.0	0.1368	–	−65.7	42.9	R

Table 4 (continued)

China, Weinan, 34.2° N, 109.2° E

Height (cm)	#	Dec.	Inc.	Rel. int.	α_{95}	Lat. (° N)	Long. (° E)	Pol.
37.0	1	−190.0	−27.0	0.1972	–	−68.1	136.1	R
39.0	1	−148.0	−60.0	0.3866	–	−63.9	354.9	R
41.0	1	−163.0	−47.0	0.3953	–	−74.3	37.0	R
43.0	1	−157.0	−37.0	0.2201	–	−65.6	47.0	R
45.0	1	−189.5	−44.8	0.4182	–	−78.7	158.2	R
48.0	1	−208.1	−12.7	0.2274	–	−52.0	158.7	I
48.5	1	−180.0	−27.9	0.2405	–	−70.6	109.2	R
49.0	1	−192.7	−49.8	0.2648	–	−78.7	184.2	R
50.0	1	−187.8	−46.3	0.2317	–	−80.6	156.8	R
51.0	1	−181.5	−48.9	0.3199	–	−85.4	125.8	R
52.0	1	−166.2	−45.7	0.2522	–	−76.2	46.3	R
53.0	1	−178.3	−44.3	0.4046	–	−81.7	98.6	R
54.0	1	−180.0	−39.7	0.3797	–	−78.3	109.2	R
55.0	1	−180.4	−44.2	0.3028	–	−81.7	111.7	R
56.0	1	−139.2	−50.0	0.1777	–	−55.6	13.3	R
57.0	1	−176.6	−47.9	0.1344	–	−84.0	79.4	R
58.0	1	−162.5	−26.1	0.1154	–	−64.1	67.2	R
58.5	1	−199.1	1.3	0.0283	–	−50.8	140.4	I
59.5	1	−198.5	9.3	0.0266	–	−47.4	137.0	I
60.0	1	−204.8	14.1	0.0287	–	−42.4	143.5	I
60.5	1	−203.5	1.0	0.0478	–	−48.9	146.5	I
61.5	1	−197.4	53.8	0.0183	–	−19.5	124.4	I
62.5	1	−165.6	33.1	0.0546	–	−36.0	92.2	I
64.0	1	−46.5	82.3	0.0482	–	43.7	94.0	I
64.5	1	118.3	62.1	0.0320	–	5.8	149.2	I
67.0	1	162.4	−38.5	0.1732	–	−70.1	164.8	R
68.0	1	174.4	−32.4	0.2922	–	−72.7	127.4	R
69.0	1	167.0	−1.1	0.1376	–	−54.2	131.8	I
70.0	1	167.0	−24.9	0.1613	–	−65.8	141.5	R
71.0	1	177.4	−43.8	0.3657	–	−81.1	124.6	R
72.0	1	184.0	−35.6	0.2740	–	−75.1	94.4	R
73.0	1	199.0	−44.8	0.2588	–	−71.9	39.6	R
74.0	1	191.5	−36.8	0.1533	–	−72.9	69.7	R
75.0	1	167.9	−21.6	0.1496	–	−64.5	137.7	R
76.0	1	189.0	−48.4	0.1543	–	−81.0	48.9	R
77.0	1	215.9	−64.1	0.1943	–	−60.5	345.1	R
78.0	1	185.0	−12.9	0.1943	–	−61.9	98.6	R
79.0	1	183.0	−28.1	0.2443	–	−70.6	100.5	R
80.0	1	181.1	−29.0	0.1927	–	−71.3	105.9	R
81.0	1	198.9	−13.5	0.1008	–	−57.6	72.4	R
82.0	1	179.8	−21.4	0.1033	–	−66.9	109.7	R
83.0	1	−33.1	73.0	0.1276	–	57.2	77.4	N
83.5	1	−103.0	71.0	0.1039	–	20.9	72.9	I
84.0	1	−53.2	63.4	0.1149	–	48.4	50.6	I
85.0	1	−20.2	52.6	0.1301	–	73.2	21.4	N
86.0	1	7.3	63.6	0.1345	–	77.7	134.0	N
87.0	1	5.6	48.5	0.0873	–	83.3	242.5	N
89.0	1	134.2	62.4	0.0854	–	−1.6	140.4	I
90.0	1	−143.0	48.2	0.1071	–	−17.6	75.8	I
91.0	1	−168.0	62.7	0.1897	–	−11.0	100.5	I
92.0	1	−170.0	51.1	0.0604	–	−23.3	99.9	I
93.0	1	−6.0	41.1	0.0732	–	78.1	317.0	N
94.0	1	−12.8	−26.5	0.1715	–	40.3	305.6	T

Table 4 (continued)

China. Weinan, 34.2° N, 109.2° E

Height (cm)	#	Dec.	Inc.	Rel. int.	α_{95}	Lat. (° N)	Long. (° E)	Pol.
95.0	1	0.0	−16.7	0.0841	–	47.3	289.2	T
96.0	1	4.5	−16.1	0.1118	–	47.4	282.6	T
97.0	1	16.0	−33.0	0.1090	–	35.6	270.4	T
99.0	1	174.7	−36.5	0.1282	–	−75.3	129.2	R
100.0	1	168.2	39.2	0.1092	–	−32.5	122.2	T
101.0	1	152.2	−17.8	0.0754	–	−54.2	161.2	T
102.0	1	205.9	66.9	0.0396	–	−3.2	92.7	T
103.0	1	194.3	48.6	0.0547	–	−24.8	95.5	T
104.0	1	189.7	38.0	0.0663	–	−33.7	98.3	T
105.0	1	75.7	73.4	0.0622	–	36.0	147.0	T
106.0	1	190.0	46.2	0.0977	–	−27.5	99.2	T
107.0	1	21.0	56.6	0.1909	–	72.7	183.3	N
108.0	1	30.8	50.6	0.1570	–	64.0	196.9	N
109.0	1	6.9	58.4	0.1543	–	82.6	155.7	N
110.0	1	8.6	53.4	0.2456	–	82.9	198.8	N
111.0	1	7.9	65.1	0.2195	–	75.8	131.6	N
112.0	1	4.4	62.6	0.1993	–	79.7	127.1	N
113.0	1	16.5	54.3	0.2443	–	76.4	191.9	N
114.0	1	22.4	52.4	0.2024	–	71.3	196.6	N
115.0	1	1.7	56.2	0.1881	–	87.1	137.2	N
116.0	1	−0.5	62.8	0.1961	–	80.0	107.1	N
117.0	1	25.6	53.7	0.1989	–	68.9	191.8	N
119.0	1	−2.4	49.0	0.3984	–	85.2	315.2	N
121.0	1	8.7	52.8	0.6247	–	82.7	203.3	N
123.0	1	18.7	48.7	0.4410	–	73.5	210.1	N
125.0	1	17.8	58.0	0.4751	–	75.0	176.7	N
127.0	1	21.6	51.5	0.4950	–	71.8	199.6	N
129.0	1	11.5	49.9	0.5197	–	79.7	215.9	N
131.0	1	0.1	58.0	0.5459	–	85.5	110.2	N
133.0	1	7.8	59.7	0.5970	–	81.1	151.2	N
133.0	1	7.8	59.7	0.5970	–	81.1	151.2	N
135.0	1	4.8	57.8	0.4867	–	84.3	150.1	N
137.0	1	11.1	60.4	0.4416	–	78.7	156.7	N
138.0	1	1.5	58.0	0.3991	–	85.4	123.9	N
140.0	1	16.0	58.0	0.3815	–	76.4	175.4	N
142.0	1	15.5	61.0	0.4902	–	75.5	161.8	N
144.0	1	9.8	54.4	0.4907	–	81.9	191.3	N
146.0	1	−2.1	51.8	0.6301	–	87.5	334.6	N
148.0	1	4.6	54.7	0.5472	–	86.1	182.7	N
150.0	1	−11.4	58.4	0.5593	–	79.6	50.7	N
152.0	1	−2.1	57.7	0.3859	–	85.5	87.6	N
154.0	1	5.5	61.8	0.3820	–	80.2	133.6	N
157.0	1	11.7	54.5	0.5883	–	80.3	191.0	N
159.0	1	2.5	58.1	0.4865	–	85.0	132.2	N
161.0	1	2.5	49.8	0.5376	–	85.8	258.1	N
163.0	1	14.6	56.4	0.7654	–	77.8	181.9	N
165.0	1	2.5	58.5	0.4801	–	84.6	130.3	N
167.0	1	12.0	54.5	0.4726	–	80.1	191.0	N
169.0	1	11.0	64.0	0.3754	–	75.8	142.0	N
171.0	1	12.0	58.0	0.4449	–	79.4	170.9	N
173.0	1	26.0	63.0	0.5707	–	67.6	164.2	N
175.0	1	−4.0	45.0	0.4478	–	81.6	314.6	N

All angular measurements in degrees. # denotes the number of samples taken per stratigraphic level. The polarity states are denoted (R) reverse. (N) normal, (I) intermediate, (T) transitional.

Table 5
Data of MBD97

Japan, Boso Heizogawa, 35.2° N, 140.2° E

Depth (cm)	#	Dec.	Inc.	Rel. int.	α_{95}	Lat. (° N)	Long. (° E)	Pol.
−258.2	1	−142.1	−25.8	–	0.0	−49.7	72.9	I
−254.7	3	−83.8	−12.3	–	44.6	1.4	41.5	I
−252.1	1	−83.2	19.0	–	0.0	11.1	54.4	I
−249.3	4	86.1	−57.5	–	30.2	−18.2	264.5	I
−247.7	1	−54.9	2.7	–	0.0	28.9	29.3	I
−244.9	3	−101.6	−8.4	–	46.4	−11.9	53.4	I
−241.4	3	−70.9	0.0	–	80.7	15.5	38.9	I
−237.8	3	−50.1	62.9	–	35.7	51.0	79.4	I
−235.0	2	−5.4	54.9	–	15.4	85.6	54.6	N
−233.5	1	−43.2	54.8	–	0.0	55.0	63.2	I
−231.1	3	−12.4	57.3	–	42.0	79.7	69.2	N
−228.1	2	−143.6	64.5	–	53.1	−2.1	116.0	T
−223.9	3	−78.5	70.3	–	81.8	34.3	96.5	T
−221.0	2	−222.1	−2.9	–	83.2	−38.4	198.9	T
−217.7	3	−218.1	−15.6	–	31.2	−45.8	201.4	T
−214.1	4	−200.1	−16.4	–	22.0	−57.5	179.4	R
−209.6	3	−200.6	−11.4	–	16.8	−54.9	177.8	I
−206.3	3	−179.6	−26.4	–	8.8	−68.8	139.1	R
−202.5	3	−166.9	−27.0	–	22.2	−66.0	107.6	R
−198.6	3	−171.6	−27.7	–	25.8	−68.2	117.8	R
−195.1	3	−172.6	−28.7	–	10.3	−69.0	120.0	R
−191.5	3	−140.9	−17.4	–	14.5	−45.7	77.0	I
−187.9	3	−150.4	−11.5	–	16.0	−49.9	90.5	I
−185.0	2	−131.7	15.9	–	75.4	−27.2	84.0	I
−182.0	3	−152.9	−5.0	–	17.8	−48.8	96.5	I
−179.8	1	−167.3	1.0	–	0.0	−52.4	119.1	I
−177.6	2	−154.0	−17.3	–	12.4	−54.5	91.9	I
−174.6	3	−118.0	35.0	–	31.7	−9.9	82.4	I
−172.8	1	−164.2	23.8	–	0.0	−40.1	119.8	I
−170.8	2	−139.8	−1.2	–	49.3	−39.0	83.9	I
−167.8	2	−168.1	20.5	–	23.4	−42.9	124.1	I
−165.5	1	−181.8	5.6	–	0.0	−51.9	143.1	I
−162.7	3	−151.0	−5.6	–	43.9	−47.9	94.0	I
−160.4	2	−181.9	−7.8	–	30.0	−58.7	143.8	R
−158.1	2	−164.0	0.8	–	36.7	−51.4	114.0	I
−156.0	2	−160.0	8.1	–	15.2	−46.5	110.5	I
−152.4	1	−169.2	10.5	–	0.0	−48.3	123.9	I
−150.1	3	−178.8	−20.8	–	14.9	−65.6	137.4	R
−146.6	3	−179.1	−20.6	–	19.4	−65.4	138.2	R
−142.6	3	−186.2	1.7	–	21.3	−53.5	150.7	T
−138.9	3	−192.7	29.8	–	43.1	−37.4	155.7	T
−136.3	3	−189.3	4.5	–	37.7	−51.6	155.3	T
−132.8	6	−196.0	30.1	–	23.8	−36.4	159.4	T
−129.1	6	−196.6	21.3	–	28.9	−41.2	162.0	T
−125.9	2	−221.7	22.8	–	12.5	−28.6	188.0	T
−123.7	2	−21.0	81.8	–	29.1	49.8	131.4	T
−120.3	3	−16.2	85.9	–	19.1	43.0	137.1	T
−118.4	1	−203.9	82.7	–	0.0	21.9	146.4	T
−115.7	3	−5.1	70.6	–	14.2	70.0	131.6	N
−112.7	3	−9.3	68.4	–	8.5	72.3	120.9	N
−109.4	2	13.6	74.1	–	19.0	63.4	155.4	N

Table 5 (continued)

Japan, Boso Heizogawa, 35.2° N, 140.2° E

Depth (cm)	#	Dec.	Inc.	Rel. int.	α_{95}	Lat. (° N)	Long. (° E)	Pol.
−105.6	3	−11.1	76.7	–	7.2	59.8	130.8	N
−103.0	2	−39.3	79.9	–	2.8	49.0	121.4	I
−100.7	2	−17.7	72.8	–	4.9	64.1	118.7	N
−97.5	3	−14.9	77.2	–	10.8	58.5	128.5	N
−93.2	4	−38.7	76.5	–	7.8	52.7	113.7	I
−89.7	2	−25.5	72.4	–	18.4	61.8	111.0	N
−87.5	2	−33.0	64.6	–	13.0	62.9	84.8	N
−84.3	3	−40.3	60.6	–	9.1	58.1	74.1	N
−82.1	1	−24.3	47.8	–	0.0	68.5	40.0	N
−79.7	2	−17.2	62.9	–	7.1	74.0	90.0	N
−75.2	3	−30.3	51.4	–	13.2	64.7	51.9	N
−72.4	4	−20.6	58.8	–	7.4	73.1	71.2	N
−69.3	2	−24.6	54.4	–	6.5	69.9	56.7	N
−65.7	3	−20.8	51.6	–	8.0	72.5	46.5	N
−62.0	3	−18.2	50.8	–	9.6	74.4	41.7	N
−58.6	3	−24.3	50.6	–	8.8	69.4	46.4	N
−55.7	3	−14.1	57.3	–	7.2	78.3	68.0	N
−52.1	2	−8.6	56.2	–	2.4	82.9	65.3	N
−49.0	3	−12.1	61.3	–	9.6	78.2	91.2	N
−45.8	2	−14.1	49.6	–	8.3	77.2	32.1	N
−44.3	1	−23.4	63.1	–	0.0	69.8	85.1	N
−42.3	2	−16.7	48.3	–	12.2	74.7	32.1	N
−39.1	3	−9.4	54.2	–	12.8	82.3	49.6	N
−35.9	2	−0.9	49.5	–	11.3	85.1	329.4	N
−32.2	3	−16.1	45.7	–	10.7	74.1	24.3	N
−28.6	3	−22.3	44.8	–	14.2	69.0	31.7	N
−24.9	3	−4.3	47.6	–	13.1	82.6	350.7	N
−21.6	3	−20.9	49.8	–	7.3	71.9	41.3	N
−16.4	3	−20.7	51.1	–	7.1	72.4	44.9	N
−14.4	2	−5.2	46.7	–	19.5	81.5	352.8	N
−10.7	3	−5.4	49.1	–	6.1	83.1	3.0	N
−6.8	3	−9.8	53.2	–	4.3	81.8	42.6	N
−2.2	2	−12.2	56.9	–	6.7	79.9	66.8	N
−232.2	1	168.4	−28.4	–	0.0	−67.4	170.4	R
−228.8	3	163.3	−8.8	–	24.0	−55.6	170.6	R
−225.8	2	190.8	−38.7	–	11.7	−73.6	101.9	R
−222.2	3	176.3	−14.3	–	19.1	−61.8	148.0	R
−220.4	1	148.8	−38.1	–	0.0	−59.5	211.7	R
−217.8	3	118.3	−13.3	–	79.3	−26.9	218.9	I
−213.1	3	162.2	3.9	–	41.2	−49.3	168.2	I
−209.7	2	113.0	1.7	–	63.3	−18.1	215.7	I
−207.3	2	93.6	27.2	–	55.8	5.4	216.4	I
−205.0	1	143.7	−18.0	–	0.0	−47.9	200.9	I
−202.1	3	−191.0	−31.2	–	12.0	−69.2	171.2	R
−198.6	2	−192.4	−26.6	–	13.4	−66.1	171.1	R
−197.0	1	−182.6	−34.2	–	0.0	−73.4	148.9	R
−193.6	3	−170.4	−36.1	–	69.8	−72.6	108.5	R
−191.2	1	−173.1	−41.5	–	0.0	−77.2	110.5	R
−188.8	2	−172.1	−39.0	–	13.6	−75.1	110.6	R
−186.4	2	−175.1	−30.9	–	12.2	−70.9	125.6	R

Table 5 (continued)

Japan, Boso Heizogawa, 35.2° N, 140.2° E

Depth (cm)	#	Dec.	Inc.	Rel. int.	α_{95}	Lat. (° N)	Long. (° E)	Pol.
−185.2	1	−165.8	−18.6	–	0.0	−61.2	110.0	R
−182.3	4	−163.9	−29.6	–	7.1	−65.9	99.5	R
−179.3	2	−173.0	−36.4	–	7.1	−73.8	115.9	R
−176.1	3	−162.6	−34.5	–	12.9	−67.7	92.2	R
−172.7	3	−161.6	−32.2	–	6.0	−65.9	92.8	R
−169.5	3	−166.7	−17.1	–	19.3	−60.9	112.4	R
−166.0	3	−163.5	−2.2	–	21.2	−52.6	112.4	I
−162.9	3	−175.7	−20.1	–	10.6	−64.9	130.3	R
−159.6	3	−181.5	−24.3	–	13.8	−67.5	144.1	R
−152.4	3	−186.5	−30.0	–	11.6	−70.0	158.7	R
−149.1	3	−176.8	−26.4	–	11.1	−68.5	131.7	R
−145.8	5	−180.8	−22.7	–	8.6	−66.6	142.1	R
−144.3	1	−202.0	−21.9	–	0.0	−58.9	185.5	R
−141.8	4	−184.2	−21.5	–	17.1	−65.6	150.3	R
−137.5	3	−187.0	−8.1	–	21.0	−58.2	153.6	R
−136.2	1	−191.2	−6.2	–	0.0	−56.3	160.6	R
−132.8	3	−196.5	12.4	–	18.3	−45.7	164.1	I
−130.0	2	−198.0	3.8	–	8.9	−49.3	168.4	I
−127.5	2	−178.5	−8.3	–	16.5	−59.0	137.3	R
−124.6	3	−183.6	−13.8	–	13.5	−61.6	147.6	R
−121.1	3	−172.9	−14.9	–	9.2	−61.6	125.2	R
−118.4	3	−177.3	12.2	–	18.5	−48.6	136.2	T
−115.0	2	−179.5	16.9	–	16.3	−46.2	139.4	T
−113.3	1	−168.9	24.8	–	0.0	−40.6	125.9	T
−110.7	3	−159.8	44.0	–	16.5	−26.1	120.0	T
−106.8	4	5.2	77.8	–	13.5	58.4	144.1	N
−104.3	2	21.4	77.2	–	12.2	57.0	156.3	N
−100.3	3	0.7	63.7	–	6.1	79.9	142.9	N
−97.1	3	−3.9	69.2	–	9.6	72.3	132.4	N
−93.1	3	−82.4	75.6	–	15.8	34.2	106.9	I
−89.6	3	−30.3	73.3	–	10.3	59.0	109.8	N
−85.7	3	−24.3	64.2	–	3.4	68.8	87.9	N
−82.1	3	−8.6	74.4	–	19.0	63.8	130.7	N
−78.9	3	−21.1	64.9	–	5.4	70.4	92.9	N
−75.3	3	−24.9	63.5	–	5.8	68.7	85.4	N
−71.6	3	−28.2	65.9	–	8.4	65.5	90.8	N
−68.6	2	−32.9	60.0	–	3.3	63.6	72.6	N
−66.7	1	−23.9	61.9	–	0.0	69.9	80.8	N
−64.1	3	−9.4	55.8	–	2.7	82.3	61.6	N
−60.5	3	−11.1	53.2	–	5.1	80.7	44.7	N
−57.4	2	−3.4	47.9	–	3.0	83.1	345.9	N
−55.7	1	−11.2	55.5	–	0.0	80.9	58.9	N
−52.9	1	6.4	56.6	–	0.0	84.4	207.0	N
−49.0	3	−4.0	56.7	–	12.7	86.2	83.6	N
−46.1	3	−4.5	56.3	–	13.0	86.0	76.0	N
−42.1	3	6.5	55.1	–	6.9	84.7	223.9	N
−38.1	3	2.0	54.4	–	12.3	88.4	239.2	N
−34.4	3	−3.3	56.9	–	11.7	86.5	92.7	N
−31.2	3	−11.0	55.0	–	11.0	81.1	55.6	N
−28.3	2	−20.7	57.0	–	11.4	73.2	64.4	N

Table 5 (continued)

Japan, Boso Heizogawa, 35.2° N, 140.2° E

Depth (cm)	#	Dec.	Inc.	Rel. int.	α_{95}	Lat. (° N)	Long. (° E)	Pol.
−25.2	3	−28.3	54.9	–	10.2	67.0	59.1	N
−21.7	3	−14.0	57.0	–	10.9	78.5	66.2	N
−18.2	4	−17.5	59.1	–	18.3	75.3	74.2	N
−15.3	1	−9.7	61.5	–	0.0	79.4	97.5	N
−12.3	5	−35.1	69.1	–	15.5	59.7	96.2	N
−9.6	3	−12.4	59.6	–	11.1	78.9	82.0	N
−6.2	3	−9.5	71.6	–	21.0	67.9	126.2	N
−1.8	4	−27.9	72.7	–	13.3	60.6	110.0	N

All angular measurements in degrees. # denotes the number of samples taken per stratigraphic level. The polarity states are denoted (R) reverse, (N) normal, (I) intermediate, (T) transitional.

Table 6
Data of MBD97

New Zealand, Wanganui, −40.0° N, 175.0° E

Height (cm)	#	Dec.	Inc.	Rel. int.	α_{95}	Lat. (° N)	Long. (° E)	Pol.
5300.0	?	197.9	32.7	–	?	−62.9	35.0	R
5500.0	?	191.4	33.9	–	?	−66.4	22.9	R
5900.0	?	149.1	44.3	–	?	−60.8	284.1	R
5990.0	?	182.5	35.3	–	?	−69.4	1.7	R
6100.0	?	184.9	33.5	–	?	−67.9	7.4	R
6140.0	?	163.1	47.1	–	?	−71.8	299.9	R
6200.0	?	240.9	−31.9	–	?	−9.5	52.8	T
6500.0	?	182.9	−48.6	–	?	−20.4	357.7	T
6850.0	?	−112.7	−48.2	–	?	3.2	48.7	T
7150.0	?	−89.4	−48.7	–	?	19.0	61.8	T
7400.0	?	155.7	−32.9	–	?	−27.8	328.7	T
7950.0	?	17.2	−71.8	–	?	69.9	326.8	N

Atlantic, 609B, 49.9° N, 335.8° E

Depth (cm)	#	Dec.	Inc.	Rel. int.	α_{95}	Lat. (° N)	Long. (° E)	Pol.
−57.5	1	−207.6	−55.2	0.7050	–	−65.5	41.0	R
−57.0	1	−202.6	−53.3	0.4250	–	−66.9	30.3	R
−56.5	1	−193.7	−57.9	0.7500	–	−75.1	21.7	R
−56.0	1	−187.2	−61.3	0.6210	–	−81.0	12.2	R
−55.5	1	−187.3	−61.3	0.7190	–	−81.0	12.6	R
−55.0	1	−193.6	−60.0	0.6360	–	−76.9	27.6	R
−54.5	1	−193.1	−60.2	0.7120	–	−77.4	27.0	R
−54.0	1	−195.1	−59.3	0.8820	–	−75.6	28.9	R
−53.5	1	−188.2	−64.4	0.8230	–	−83.4	35.3	R
−53.0	1	−191.0	−57.4	1.0000	–	−75.8	13.5	R
−52.5	1	−197.5	−64.5	0.8050	–	−77.8	55.7	R
−52.0	1	−208.8	−66.7	0.5770	–	−71.4	75.0	R
−51.5	1	−208.8	−68.2	0.5740	–	−71.8	81.5	R
−51.0	1	−192.6	−67.0	0.4430	–	−81.9	69.3	R
−50.5	1	−191.4	−67.5	0.4460	–	−82.7	74.1	R
−50.0	1	−192.2	−67.5	0.4360	–	−82.2	74.1	R
−49.5	1	−195.3	−67.8	0.4300	–	−80.2	77.0	R
−49.0	1	−203.7	−64.9	0.3530	–	−74.0	64.1	R

Table 6 (continued)

Atlantic, 609B, 49.9° N, 335.8° E

Depth (cm)	#	Dec.	Inc.	Rel. int.	α_{95}	Lat. (° N)	Long. (° E)	Pol.
−48.5	1	−207.3	−68.3	0.4380	–	−72.7	81.7	R
−48.0	1	−205.4	−66.0	0.4050	–	−73.4	70.2	R
−47.5	1	−196.2	−65.2	0.3850	–	−79.0	58.3	R
−47.0	1	−179.8	−68.5	0.3200	–	−88.1	159.5	R
−46.5	1	−190.4	−66.8	0.3090	–	−83.3	65.5	R
−46.0	1	−189.2	−66.5	0.3060	–	−84.0	61.0	R
−45.5	1	−186.5	−67.7	0.3530	–	−85.8	78.9	R
−45.0	1	−184.2	−67.2	0.2900	–	−87.3	69.2	R
−44.5	1	−183.2	−65.3	0.3810	–	−86.7	17.5	R
−44.0	1	−190.6	−62.6	0.3870	–	−80.7	30.6	R
−43.5	1	−188.6	−61.3	0.4770	–	−80.5	17.6	R
−43.0	1	−182.1	−62.6	0.4690	–	−83.9	350.2	R
−42.5	1	−185.4	−64.2	0.4070	–	−84.7	20.7	R
−42.0	1	−184.1	−63.2	0.3360	–	−84.1	5.7	R
−41.5	1	−182.6	−62.5	0.2680	–	−83.7	353.2	R
−41.0	1	−193.1	−61.8	0.2700	–	−78.7	33.4	R
−40.5	1	−194.9	−71.0	0.0750	–	−79.4	103.3	R
−40.0	1	−223.7	−67.8	0.3020	–	−62.5	84.7	R
−39.5	1	−218.0	−66.5	0.2580	–	−65.5	78.5	R
−39.0	1	−223.7	−65.3	0.2200	–	−61.4	77.9	R
−38.5	1	−224.2	−66.2	0.2160	–	−61.5	80.5	R
−38.0	1	−232.9	−62.1	0.1760	–	−53.9	76.3	I
−37.5	1	−227.2	−58.2	0.2020	–	−55.2	65.8	R
−37.0	1	−227.5	−59.9	0.2380	–	−56.0	68.8	R
−36.5	1	−214.4	−53.2	0.2470	–	−60.1	46.3	R
−36.0	1	−216.9	−58.1	0.1160	–	−61.7	56.9	R
−35.5	1	−230.4	−64.0	0.0940	–	−56.5	78.5	R
−35.0	1	−183.8	−63.1	0.0510	–	−84.1	3.2	R
−34.5	1	−194.4	−21.8	0.0540	–	−49.7	357.9	I
−34.0	1	−188.8	−56.9	0.0990	–	−76.1	6.1	R
−33.5	1	−174.7	−73.4	0.1550	–	−80.2	171.9	R
−33.0	1	−173.4	−76.9	0.1640	–	−74.4	166.2	R
−32.0	1	−186.4	−70.2	0.1600	–	−84.1	116.3	R
−31.5	1	−186.2	−56.5	0.1530	–	−76.5	357.4	R
−31.0	1	−176.0	−50.8	0.1370	–	−71.4	325.0	R
−30.0	1	−185.7	−52.1	0.1630	–	−72.3	351.8	R
−29.5	1	−179.9	−55.5	0.1770	–	−76.2	335.4	R
−29.0	1	−177.6	−51.6	0.1640	–	−72.3	329.1	R
−28.5	1	−182.0	−48.7	0.2200	–	−69.7	340.8	R
−28.0	1	−189.1	−48.0	0.1900	–	−68.1	357.5	R
−27.5	1	−190.2	−53.3	0.1770	–	−72.3	4.7	R
−27.0	1	−182.6	−45.3	0.1770	–	−66.9	341.7	R
−26.5	1	−185.9	−43.7	0.1710	–	−65.3	348.6	R
−26.0	1	−180.7	−43.5	0.1680	–	−65.5	337.3	R
−25.5	1	−172.9	−33.6	0.1280	–	−58.0	323.0	R
−24.5	1	−162.3	−11.8	0.0900	–	−43.6	311.1	T
−24.0	1	−156.6	5.7	0.0430	–	−33.6	307.3	T
−23.5	1	−157.1	8.6	0.0630	–	−32.3	308.4	T
−22.0	1	−108.1	43.8	0.0280	–	8.6	275.7	T
−21.5	1	−77.5	70.4	0.0360	–	44.7	282.9	T
−21.1	1	−42.5	55.6	0.0630	–	56.6	237.9	N

Table 6 (continued)

Atlantic, 609B, 49.9° N, 335.8° E

Depth (cm)	#	Dec.	Inc.	Rel. int.	α_{95}	Lat. (° N)	Long. (° E)	Pol.
−20.0	1	15.4	60.2	0.0420	–	76.2	99.0	N
−19.5	1	1.3	22.6	0.0730	–	51.9	153.7	I
−19.0	1	−34.1	16.3	0.1050	–	39.7	201.9	I
−18.5	1	−37.7	12.4	0.1710	–	36.2	204.6	I
−18.0	1	−50.9	−9.0	0.0700	–	20.2	211.3	I
−17.5	1	−32.1	13.6	0.1170	–	39.3	198.8	I
−17.0	1	−27.1	−2.1	0.1060	–	34.0	189.1	I
−16.5	1	−13.9	17.1	0.0860	–	47.3	176.3	I
−16.0	1	−21.3	1.0	0.0930	–	37.4	183.0	I
−15.5	1	−22.9	28.0	0.1020	–	50.4	191.9	I
−15.0	1	−17.7	30.5	0.1100	–	53.6	185.2	I
−14.5	1	−22.7	21.5	0.0800	–	47.0	189.5	I
−14.0	1	−1.9	39.0	0.1500	–	62.1	159.5	N
−13.5	1	0.2	42.8	0.1660	–	65.0	155.3	N
−13.0	1	−24.7	39.3	0.0380	–	56.3	199.9	N
−12.5	1	9.6	42.0	0.1670	–	63.3	136.0	N
−12.0	1	−55.1	87.4	0.2140	–	52.6	328.8	I
−11.5	1	19.6	51.2	0.2020	–	66.8	109.4	N
−11.0	1	16.5	48.4	0.1390	–	66.0	118.3	N
−10.5	1	45.5	67.1	0.0230	–	61.1	48.1	N
−10.0	1	35.0	49.1	0.1180	–	57.1	89.7	N
−9.5	1	41.6	46.2	0.0900	–	51.3	85.3	I
−9.0	1	47.5	54.8	0.0910	–	52.9	70.4	I
−8.5	1	46.0	47.6	0.0800	–	49.5	79.7	I
−8.5	1	47.1	60.5	0.0820	–	56.6	61.9	N
−8.0	1	37.1	71.8	0.1380	–	67.1	34.2	N
−7.5	1	−34.4	74.4	0.1030	–	67.9	288.6	N
−7.0	1	54.2	87.0	0.1000	–	53.1	343.9	I
−6.0	1	4.2	80.0	0.1540	–	69.2	339.7	N
−5.5	1	−102.6	75.6	0.0880	–	38.0	301.3	I
−5.0	1	−114.1	81.2	0.1070	–	40.7	314.9	I
−4.5	1	−31.5	69.6	0.1330	–	70.3	268.1	N
−4.0	1	−19.3	69.5	0.1050	–	77.6	268.8	N
−3.5	1	−3.4	64.9	0.1500	–	86.3	194.1	N
−3.0	1	15.1	66.2	0.1990	–	80.1	67.4	N
−2.5	1	−260.6	85.0	0.0900	–	47.3	350.3	I
−2.0	1	−19.5	81.9	0.0640	–	64.4	323.6	N
−1.5	1	−8.2	87.7	0.0890	–	54.4	334.6	I

All angular measurements in degrees. # denotes the number of samples taken per stratigraphic level. The polarity states are denoted (R) reverse, (N) normal, (I) intermediate, (T) transitional.

Table 7
Data of MBD97

Atlantic, 664D, 0.1° N, 336.7° E

Depth (cm)	#	Dec.	Inc.	Rel. int.	α_{95}	Lat. (° N)	Long. (° E)	Pol.
−146.0	1	174.1	17.0	1.0000	–	−79.4	10.3	R
−145.0	1	175.1	18.5	–	–	−79.2	3.5	R
−144.0	1	180.9	22.7	0.9600	–	−78.1	332.5	R

Table 7 (continued)

Atlantic, 664D, 0.1° N, 336.7° E								
Depth (cm)	#	Dec.	Inc.	Rel. int.	α_{95}	Lat. (° N)	Long. (° E)	Pol.
−143.0	1	175.9	21.6	–	–	−78.0	356.4	R
−142.0	1	171.7	14.6	0.9400	–	−78.8	24.3	R
−141.0	1	167.9	30.1	–	–	−69.8	12.4	R
−140.0	1	177.4	26.7	0.8800	–	−75.6	346.9	R
−139.0	1	165.3	20.1	–	–	−72.0	30.7	R
−138.0	1	182.0	14.3	–	–	−82.4	321.6	R
−137.0	1	186.9	21.4	0.5800	–	−76.9	305.4	R
−136.0	1	203.4	29.7	–	–	−61.9	282.6	R
−135.0	1	194.6	24.8	0.4800	–	−70.5	289.4	R
−134.0	1	191.9	21.9	–	–	−73.5	291.2	R
−133.0	1	188.0	42.6	0.4800	–	−64.0	319.9	R
−132.0	1	193.6	26.2	–	–	−70.6	293.2	R
−131.0	1	176.8	25.4	0.5000	–	−76.2	349.9	R
−130.0	1	176.4	15.3	–	–	−81.3	1.1	R
−129.0	1	161.5	21.1	0.9400	–	−68.6	35.2	R
−128.0	1	175.7	26.2	–	–	−75.4	353.6	R
−127.0	1	188.5	21.7	0.7800	–	−75.8	300.4	R
−126.0	1	172.4	20.9	–	–	−76.7	11.2	R
−125.0	1	174.6	41.0	0.7000	–	−65.8	348.9	R
−124.0	1	166.2	34.6	–	–	−66.6	11.3	R
−123.0	1	160.5	30.6	0.4400	–	−64.6	25.0	R
−122.0	1	144.7	44.6	–	–	−47.0	26.2	I
−121.0	1	149.1	54.9	0.3400	–	−44.3	12.5	I
−120.0	1	150.9	29.6	–	–	−57.1	36.3	R
−119.0	1	169.5	26.1	–	–	−72.7	13.2	R
−118.0	1	186.7	43.4	–	–	−63.8	322.9	R
−117.0	1	178.9	6.2	0.4800	–	−86.6	355.6	R
−116.0	1	144.4	3.9	–	–	−54.3	63.2	I
−114.0	1	157.5	1.2	0.3600	–	−67.5	64.9	R
−113.0	1	176.4	9.9	–	–	−83.8	11.9	R
−112.0	1	160.4	12.0	0.3600	–	−69.5	48.9	R
−111.0	1	178.4	1.7	–	–	−88.1	36.0	R
−110.0	1	157.9	16.9	0.4200	–	−66.3	44.5	R
−109.0	1	171.3	−6.8	–	–	−80.7	87.7	R
−108.0	1	168.7	−4.1	0.6800	–	−78.5	76.6	R
−103.0	1	178.1	6.4	0.4400	–	−86.2	6.6	R
−102.0	1	177.9	0.8	0.4800	–	−87.8	53.3	R
−101.0	1	181.3	−4.5	–	–	−87.5	187.8	R
−100.0	1	187.4	−0.7	0.5200	–	−82.6	244.8	R
−99.0	1	177.4	5.5	–	–	−86.1	19.0	R
−97.0	1	194.6	−15.2	–	–	−73.6	218.7	R
−96.0	1	193.6	−13.5	0.2800	–	−74.8	220.0	R
−95.0	1	180.0	–	–	–	−89.9	336.7	R
−94.0	1	185.0	−8.3	0.1600	–	−83.6	207.5	R
−93.0	1	175.7	−22.5	–	–	−77.6	136.7	R
−92.0	1	177.0	−4.8	0.4800	–	−86.2	104.3	R
−91.0	1	179.0	5.3	–	–	−87.1	356.7	R
−90.0	1	176.0	2.3	0.4000	–	−85.8	49.4	R
−89.0	1	180.8	14.7	–	–	−82.4	330.7	R
−88.0	1	179.1	16.5	0.6200	–	−81.4	342.7	R
−86.0	1	179.0	6.6	0.5800	–	−86.4	353.1	R

Table 7 (continued)

Atlantic, 664D, 0.1° N, 336.7° E

Depth (cm)	#	Dec.	Inc.	Rel. int.	α_{95}	Lat. (° N)	Long. (° E)	Pol.
−85.0	1	169.0	i 8.1	–	–	−78.2	45.8	R
−84.0	1	186.3	3.0	–	–	−83.5	261.0	R
−83.0	1	176.9	4.2	0.8600	–	−86.2	31.3	R
−82.0	1	182.3	5.1	–	–	−86.5	295.9	R
−81.0	1	184.3	−0.9	0.4800	–	−85.7	242.1	R
−80.0	1	178.5	1.6	–	–	−88.3	35.8	R
−79.0	1	184.2	−12.9	0.3400	–	−82.3	189.7	R
−78.0	1	185.9	−7.6	–	–	−83.0	214.4	R
−77.0	1	186.5	−3.6	0.2200	–	−83.3	232.0	R
−76.0	1	176.2	9.8	–	–	−83.7	13.7	R
−75.0	1	178.0	−0.8	0.2800	–	−88.0	75.3	R
−74.0	1	175.0	−1.7	0.4600	–	−84.9	75.3	R
−73.0	1	173.5	−3.9	0.4000	–	−83.2	82.7	R
−72.0	1	171.0	−10.0	0.3200	–	−79.7	95.7	R
−70.0	1	155.0	−5.0	0.2200	–	−64.9	72.4	R
−69.0	1	185.1	5.6	–	–	−84.1	276.5	R
−68.0	1	149.0	–	0.2200	–	−59.0	66.6	R
−67.0	1	153.5	2.2	0.2000	–	−63.5	64.1	R
−66.0	1	158.0	6.7	0.1400	–	−67.7	57.6	R
−65.0	1	160.0	6.0	0.2000	–	−69.8	57.7	R
−64.0	1	160.2	6.8	0.1800	–	−69.9	56.5	R
−63.0	1	162.4	−18.3	0.1800	–	−70.2	95.2	R
−62.0	1	182.5	–	0.2000	–	−87.5	249.0	R
−61.0	1	148.1	−2.0	0.1200	–	−58.1	68.5	R
−60.0	1	115.8	−35.0	0.1200	–	−24.3	87.9	T
−59.0	1	145.1	−9.8	–	–	−54.8	75.2	T
−58.0	1	138.0	−23.0	0.0800	–	−46.7	84.2	T
−57.0	1	119.0	–	0.1000	–	−29.0	66.7	T
−56.0	1	110.7	−31.0	0.1400	–	−19.8	84.5	T
−55.0	1	117.0	−20.5	0.1000	–	−26.5	78.5	T
−53.0	1	53.0	–	0.0200	–	37.0	66.8	T
−51.0	1	43.0	−9.8	0.1000	–	46.8	74.1	T
−50.0	1	48.0	−11.0	0.0800	–	41.7	74.3	T
−49.0	1	13.0	−13.3	–	–	75.3	94.8	N
−48.0	1	44.5	−10.9	0.1000	–	45.2	74.7	I
−47.0	1	47.0	−18.4	–	–	42.3	79.6	I
−46.0	1	10.0	−34.0	–	–	68.8	129.6	N
−45.0	1	32.7	−13.7	0.1200	–	56.6	79.6	N
−44.0	1	41.0	−37.9	0.1000	–	44.6	97.5	I
−42.0	1	3.0	−9.0	0.1400	–	84.5	123.8	N
−41.0	1	5.8	−15.6	0.1200	–	80.1	121.2	N
−40.0	1	17.1	−5.4	0.2000	–	72.7	76.2	N
−39.0	1	11.0	−3.1	0.1400	–	78.9	75.3	N
−38.0	1	16.3	−3.0	0.1800	–	73.6	72.4	N
−37.0	1	20.3	−8.8	0.1200	–	69.2	79.6	N
−36.0	1	15.6	−24.1	0.1400	–	70.0	106.7	N
−35.0	1	14.3	−27.5	0.1800	–	69.6	113.4	N
−34.0	1	17.9	−31.3	–	–	65.5	111.6	N
−33.0	1	23.1	−21.4	–	–	64.5	93.5	N
−32.0	1	34.2	−29.3	0.1800	–	52.7	93.4	I
−31.0	1	31.7	−41.7	–	–	50.9	107.1	I
−30.0	1	19.1	−6.4	0.3600	–	70.6	76.7	N
−29.0	1	5.0	16.1	–	–	80.5	8.2	N

Table 7 (continued)

Atlantic, 664D, 0.1° N, 336.7° E								
Depth (cm)	#	Dec.	Inc.	Rel. int.	α_{95}	Lat. (° N)	Long. (° E)	Pol.
−28.0	1	9.1	−1.8	–	–	80.8	73.0	N
−27.0	1	8.7	−4.0	0.2400	–	81.1	80.4	N
−26.0	1	30.2	−6.2	–	–	59.6	73.1	N
−25.0	1	12.4	−3.3	0.3000	–	77.5	74.8	N
−24.0	1	1.3	−0.2	–	–	88.7	75.5	N
−23.0	1	6.2	−3.9	0.4600	–	83.5	85.1	N
−22.0	1	−3.3	4.5	–	–	86.1	279.9	N
−21.0	1	0.9	−6.5	0.5400	–	86.5	141.8	N
−20.0	1	3.6	−8.6	–	–	84.3	117.7	N
−19.0	1	1.7	−6.0	0.3800	–	86.5	128.1	N
−18.0	1	−2.4	−4.2	–	–	86.7	204.2	N
−17.0	1	2.6	−3.6	0.6000	–	86.8	102.9	N
−16.0	1	4.7	−4.7	–	–	84.7	94.3	N
−15.0	1	8.2	−5.1	–	–	81.4	84.7	N
−14.0	1	4.3	−3.7	0.7200	–	85.3	91.2	N
−13.0	1	−2.0	−2.6	0.8000	–	87.6	211.7	N
−12.0	1	−6.5	−9.1	–	–	82.0	210.9	N
−11.0	1	−11.2	−16.3	–	–	76.0	209.4	N

All angular measurements in degrees. # denotes the number of samples taken per stratigraphic level. The polarity states are denoted (R) reverse, (N) normal, (I) intermediate, (T) transitional.

Table 8
Data of MBD97

Indian, V16-58, −46.0° N, 30.0° E								
Depth (cm)	#	Dec.	Inc.	Rel. int.	α_{95}	Lat. (° N)	Long. (° E)	Pol.
−1143.4	1	−149.5	62.6	0.8859	–	−68.5	305.7	R
−1142.3	1	−183.7	60.7	0.6848	–	−84.9	176.9	R
−1141.1	1	−155.3	57.6	0.7663	–	−70.2	285.7	R
−1140.5	1	−157.2	61.1	0.4946	–	−73.2	295.0	R
−1139.9	1	−151.9	65.5	0.5326	–	−70.8	315.2	R
−1139.2	1	−146.2	65.5	0.5272	–	−67.0	316.5	R
−1138.7	1	−151.1	57.9	0.8913	–	−67.5	291.1	R
−1138.2	1	−129.7	60.8	0.6630	–	−54.1	311.9	I
−1137.6	1	−143.0	62.4	0.4348	–	−63.9	308.5	R
−1137.0	1	−116.7	72.8	0.4620	–	−50.9	341.8	I
−1136.5	1	−130.5	58.5	0.4511	–	−53.5	307.5	I
−1136.0	1	−131.0	65.8	0.5380	–	−57.1	321.7	R
−1135.5	1	−127.1	56.2	0.3207	–	−50.0	306.1	I
−1135.0	1	−149.2	64.9	0.4239	–	−68.9	313.6	R
−1134.4	1	−125.6	61.6	0.4728	–	−51.7	315.4	I
−1133.8	1	−130.3	71.7	0.2554	–	−58.0	337.5	R
−1133.3	1	−77.8	45.6	0.4293	–	−11.3	327.4	T
−1132.7	1	−131.4	43.0	0.2935	–	−46.1	288.6	T
−1132.2	1	−96.2	17.8	0.0978	–	−10.8	301.9	T
−1131.6	1	−115.2	36.0	0.1957	–	−31.6	296.6	T
−1131.1	1	−89.7	−37.7	0.1087	–	15.2	285.2	T
−1130.6	1	−78.6	−56.3	0.1304	–	32.8	278.9	T
−1130.0	1	−29.5	−46.0	0.1902	–	60.2	328.4	N
−1129.4	1	−43.2	−73.4	0.0815	–	61.3	256.9	N

Table 8 (continued)

Indian, V16-58, −46.0° N, 30.0° E

Depth (cm)	#	Dec.	Inc.	Rel. int.	α_{95}	Lat. (° N)	Long. (° E)	Pol.
−1128.8	1	−35.2	−49.2	0.1576	–	58.4	317.8	N
−1128.2	1	−72.1	−33.4	0.1087	–	25.3	299.5	I
−1127.7	1	−107.0	−27.1	0.1522	–	−1.1	277.9	I
−1127.2	1	−48.7	−42.9	0.1141	–	46.0	311.4	I
−1126.7	1	−34.8	−59.7	0.1522	–	64.3	299.6	N
−1126.1	1	6.4	−68.1	0.1576	–	83.3	173.2	N
−1125.6	1	−24.9	−70.0	0.2120	–	72.2	264.4	N
−1125.1	1	−24.4	−58.8	0.2609	–	71.1	311.2	N
−1124.6	1	−64.1	−53.3	0.2391	–	40.7	290.4	I
−1124.1	1	−21.2	−56.8	0.2337	–	72.1	321.1	N
−1123.5	1	−42.2	−30.2	0.1359	–	44.0	326.2	I
−1123.0	1	−74.5	−40.7	0.1576	–	27.0	293.7	I
−1122.4	1	−45.8	−57.0	0.2174	–	55.3	297.3	N
−1121.8	1	2.2	−73.7	0.2011	–	76.3	205.3	N
−1121.3	1	−31.9	−54.0	0.2772	–	63.3	314.1	N
−1120.8	1	−36.0	−51.2	0.1848	–	59.0	314.3	N
−1120.3	1	−49.6	−54.0	0.2120	–	51.1	299.1	I
−1119.6	1	−70.8	−56.8	0.2283	–	38.2	282.7	I
−1119.0	1	−42.2	−46.3	0.1957	–	52.1	314.2	I
−1118.5	1	−6.4	−74.0	0.2663	–	75.3	222.7	N
−1117.9	1	8.2	−61.2	0.5598	–	83.0	90.7	N
−1117.4	1	−6.6	−68.5	0.4022	–	82.8	244.5	N
−1116.9	1	−19.9	−65.6	0.3696	–	76.3	285.3	N
−1116.3	1	−28.6	−80.5	0.4620	–	61.1	228.3	N
−1115.8	1	−44.3	−61.3	0.2826	–	58.5	290.3	N
−1115.3	1	21.0	−68.9	0.2609	–	74.9	152.5	N
−1114.7	1	−5.3	−61.8	0.5000	–	85.2	336.6	N
−1114.2	1	10.3	−65.3	0.5761	–	82.8	134.8	N
−1113.6	1	22.8	−58.6	0.3533	–	72.0	106.3	N
−1113.0	1	−18.3	−60.3	0.4891	–	76.0	313.3	N
−1112.4	1	−2.9	−65.3	0.4946	–	87.6	264.0	N
−1111.9	1	−6.2	−64.8	0.6250	–	85.7	288.0	N
−1111.3	1	29.3	−67.7	0.5924	–	70.1	144.2	N
−1110.8	1	1.9	−64.4	0.7717	–	88.7	130.2	N
−1109.6	1	−6.0	−68.6	0.6141	–	82.9	241.5	N
−1108.4	1	−18.3	−68.9	0.4891	–	76.5	265.3	N
−1106.0	1	7.8	−62.3	0.5924	–	84.0	99.4	N
−1105.5	1	1.0	−59.1	0.6413	–	83.8	37.2	N
−1105.0	1	2.2	−59.8	0.6902	–	84.4	47.5	N
−1104.5	1	1.8	−65.3	0.6848	–	88.1	169.0	N
−1104.0	1	11.3	−58.6	0.7391	–	79.4	85.2	N
−1103.5	1	4.8	−56.0	0.7717	–	79.9	52.5	N
−1103.0	1	13.9	−61.1	0.9022	–	79.3	104.0	N
−1102.5	1	17.7	−62.8	0.7826	–	77.4	118.2	N
−1102.0	1	18.4	−58.9	0.8587	–	75.1	101.3	N
−1101.5	1	15.5	−63.2	1.0000	–	79.0	118.8	N
−1101.0	1	16.5	−58.3	0.9728	–	76.0	95.8	N
−1100.5	1	15.7	−60.9	1.0000	–	78.0	105.8	N
−1100.0	1	−2.8	−60.4	0.9457	–	84.9	5.5	N
−1099.5	1	−2.2	−63.2	0.7283	–	88.0	339.1	N

All angular measurements in degrees. # denotes the number of samples taken per stratigraphic level. The polarity states are denoted (R) reverse, (N) normal, (I) intermediate, (T) transitional.

References

Athanassopoulos, J., 1993. A Matuyama–Brunhes polarity reversal record: comparison between thermal and alternating field demagnetization on ocean sediments from the north Pacific Transect. PhD Thesis, University of California, Santa Barbara.

Baksi, A.K., Hsu, V., McWilliams, M.O., Farrar, E., 1992. ^{40}Ar–^{39}Ar datin of the Brunhes–Matuyama geomagnetic field reversal. Science 256, 356–357.

Barton, C.E., McFadden, P.L., 1996. Inclination shallowing and preferred transitional VGP paths. Earth Planet. Sci. Lett. 140, 147–157.

Bloxham, J., Jackson, A., 1992. Time-dependent mapping of the magnetic field at the core–mantle boundary. J. Geophys. Res. 97, 19537–19563.

Brown, L., Pickens, J., Singer, B., 1994. Matuyama–Brunhes transition recorded in lava flows of the Chilean Andes: evidence for dipolar fields during reversals. Geology 22, 299–302.

Bucha, V., 1970. Geomagnetic reversals in quaternary revealed from a paleomagnetic investigation of sedimentary rocks. J. Geomagn. Geoelectr. 22, 253–271.

Camps, P., Prévot, M., 1996. A statistical model of the fluctuations in the geomagnetic field from paleosecular variation to reversal. Science 273, 776–779.

Chauvin, A., Roperch, P., Duncan, R., 1990. Records of geomagnetic reversals from volcanic islands of French Polynesia: 2. Paleomagnetic study of a flow sequence (1.2–0.6 Ma) from the island of Tahiti and discussion of reversal models. J. Geophys. Res. 95, 2727–2752.

Cisowski, S.M., Koyama, M., 1992. Detailed record of the Brunhes–Matuyama polarity reversal in high sedimentation rate marine sediments from the Izu-Bonin Arc. Proc. Ocean Drill. Prog. Sci. Results 126, 341–352.

Clement, B.M., 1991. Geographical distribution of transitional VGPs: evidence for nonzonal equatorial symmetry during the Matuyama–Brunhes geomagnetic reversal. Earth Planet. Sci. Lett. 104, 48–58.

Clement, B.M., 1994. Geomagnetic polarity transition records from ODP cores. JOI/USSAC Workshop Rep., Florida International University.

Clement, B.M., Kent, D.V., 1984. Latitudinal dependency of geomagnetic polarity transition durations. Nature 310, 488–491.

Clement, B.M., Kent, D.V., 1986. Geomagnetic polarity transition records from five hydraulic piston core sites in the north Atlantic. Init. Rep. Deep Sea Drill. Proj. 94, 831–852.

Clement, B.M., Kent, D.V., 1991. A southern hemisphere record of the Matuyama–Brunhes polarity reversal. Geophys. Res. Lett. 18, 81–84.

Clement, B.M., Kent, D.V., Opdyke, N.D., 1982. Brunhes–Matuyama polarity transition in three deep-sea sediment cores. Philos. Trans. R. Soc. London 306, 113–119.

Dagley, P., Wilson, R.L., 1971. Geomagnetic field reversals: a link between strength and orientation of a dipole source. Nature 232, 16–18.

Egbert, G.D., 1992. Sampling bias in VGP longitudes. Geophys. Res. Lett. 19, 2353–2356.

Fuller, M., Williams, I., Hoffman, K.A., 1979. Paleomagnetic records of geomagnetic field reversals and the morphology of the transitional fields. Rev. Geophys. Space Phys. 17, 179–203.

Gubbins, D., 1994. Geomagnetic polarity reversals: a connection with secular variation and core–mantle interaction?. Rev. Geophys. 32, 61–83.

Gubbins, D., Coe, R., 1993. Longitudinally confined geomagnetic reversal paths from nondipolar transition fields. Nature 362, 51–53.

Gubbins, D., Kelly, P., 1993. Persistent patterns in the geomagnetic field during the last 2.5 Myr. Nature 365, 829–832.

Gubbins, D., Sarson, G., 1994. Geomagnetic field morphology from kinematic dynamo models. Nature 368, 51–55.

Harrison, C.G.A., Somayajulu, B.L.K., 1966. Behavior of the earth's magnetic field during a reversal. Nature 211, 1193–1195.

Hartl, P., Tauxe, L., 1996. A precursor to the Matuyama–Brunhes transition-field instability as recorded in pelagic sediments. Earth Planet. Sci. Lett. 138, 121–135.

Hillhouse, J., Cox, A., 1976. Bruhnes–Matuyama polarity transition. Earth Planet. Sci. Lett. 29, 51–64.

Hoffman, K.A., 1992. Dipolar reversal state of the geomagnetic field and core–mantle dynamics. Nature 359, 789–794.

Hoffman, K.A., Slade, S.B., 1986. Polarity transition records and the acquisition of remanence: a cautionary note. Geophys. Res. Lett. 13, 483–486.

Johnson, C.L., Constable, C.G., 1996. Paleosecular variation recorded by lava flows over the past five million years. Philos. Trans. R. Soc. London 354, 89–141.

Kawai, N., Nakajima, T., Hirooka, K., Kobayashi, K., 1973. The transition of field at the Brunhes and Jaramillo boundaries in the Matuyama geomagnetic epoch. Proc. Jpn. Acad. 49, 820–824.

Kawai, N., Otofuji, Y., Nakajima, T., Kobayashi, K., 1975. Geomagnetic stage transitional from the Matuyama to Brunhes epochs. Proc. Jpn. Acad. 51, 634–638.

Kawai, N., Sato, T., Sueishi, T., Kobayashi, K., 1977. Paleomagnetic study of deep-sea sediments using thin sections. J. Geomagn. Geoelectr. 29, 211–223.

Kent, D.V., Opdyke, N.D., 1977. Paleomagnetic field intensity variation recorded in Brunhes epoch deep-sea sediment core. Nature 266, 156–159.

Kent, D.V., Schneider, D.A., 1995. Correlation of paleointensity variation records in the Brunhes–Matuyama polarity transition interval. Earth Planet. Sci. Lett. 129, 135–144.

Kočí, A., Šibrava, V., 1976. The Brunhes–Matuyama boundary at central European localities. Quaternary Glaciations in the Northern Hemisphere. IUGS-UNESCO, pp. 135–160.

Kočí, A., Ložek, V., Małkowski, Z., 1974. Paleomagnetic investigation of the Suchdol Terrace of the River Vltava. Studia Geophys. Geod. 18, 259–265.

Kok, Y.S., Tauxe, L., 1996. Saw-toothed pattern of relative paleointensity records and cumulative viscous remanence. Earth Planet. Sci. Lett. 137, 95–99.

Knstjánsson, L., Jóhannesson, H., Eiríksson, J., Gudmundsson, A.I., 1988. Brunhes–Matuyama paleomagnetism in three lava sections in Iceland. Can. J. Earth Sci. 25, 215–225.

Laj, C., Mazaud, A., Weeks, R., Fuller, M., Herrero-Bervera, E., 1991. Geomagnetic reversal paths. Nature 351, 447.

Langereis, C.G., Hoof, A.A.M.V., Rochette, P., 1992. Longitudinal confinement of geomagnetic reversal paths as a possible sedimentary artifact. Nature 358, 226–230.

Larson, E.E., Patterson, P.E., 1993. The Matuyama–Brunhes reversal at Tecopa basin, southeastern California, revisited again. Earth Planet. Sci. Lett. 120, 311–325.

Liddicoat, J.C., 1993. Matuyama–Brunhes polarity transition near Bishop, California. Geophys. J. Int. 112, 497–506.

Lin, J.L., Verosub, K.L., Roberts, A.P., 1994. Decay of the virtual dipole moment during polarity transitions and geomagnetic excursions. Geophys. Res. Lett. 21, 525–528.

Lowes, F.J., 1975. Vector errors in spherical harmonic analysis of scalar data. Geophys. J. R. Astron. Soc. 42, 637–651.

Mazaud, A., 1996. Saw-tooth variation in magnetic intensity profiles and delayed acquisition of magnetization in deep-sea cores. Earth Planet. Sci. Lett. 139, 379–386.

McFadden, P.L., Barton, C.E., Merrill, R.T., 1993. Do virtual geomagnetic poles follow preferred paths during geomagnetic reversals?. Nature 361, 342–344.

Merrill, R.T., McElhinny, M.W., 1983. The Earth's Magnetic Field: Its History, Origin and Planetary Perspective. Academic Press, San Diego.

Meynadier, L., Valet, J.P., 1996. Post-depositional realignment of magnetic grains and asymmetrical saw-tooth patterns of magnetization intensity. Earth Planet. Sci. Lett. 140, 123–132.

Niitsuma, N., 1971. Detailed study of the sediments recording the Matuyama–Brunhes geomagnetic reversal. Tohoku Univ. Sci. Rep. 2nd Ser. Geol. 43, 1–39.

Okada, M., Niitsuma, N., 1989. Detailed paleomagnetic records during the Brunhes–Matuyama geomagnetic reversal, and a direct determination of depth lag for magnetization in marine sediments. Phys. Earth Planet. Int. 56, 133–150.

Pillans, B.J., Roberts, A.P., Wilson, G.S., Abbott, S.T., Alloway, B.V., 1994. Magnetostratigraphic, lithostatigraphic and tephrostratigraphic constraints on lower and middle Pleistocene sea-level changes, Wanganui Basin, New Zealand. Earth Planet. Sci. Lett. 121, 81–98.

Prévot, M., Camps, P., 1993. Absence of preferred longitudinal sectors for poles from volcanic records of geomagnetic reversals. Nature 366, 53–57.

Quidelleur, X., Valet, J.P., 1996. Geomagnetic changes across the last reversal recorded in lava flows from La Palma, Canary Islands. J. Geophys. Res. 101, 13755–13773.

Quidelleur, X., Valet, J.P., Courtillot, V., Hulot, G., 1994. Long-term geometry of the geomagnetic field for the last 5 million years: an updated secular variation database from volcanic sequences. Geophys. Res. Lett. 21, 1639–1642.

Roberts, A.P., Pillans, B.J., 1993. Rock magnetism of lower/middle Pleistocene marine sediments, Wanganui Basin, New Zealand. Geophys. Res. Lett. 20, 839–842.

Schneider, D.A., Kent, D.V., Mello, G.A., 1992. A detailed chronology of the Australasian impact event, the Brunhes–Matuyama geomagnetic polarity reversal, and global climate change. Earth Planet. Sci. Lett. 111, 395–405.

Schönharting, G., Sharma, P.V., Kentved, S., 1989. Magnetic polarity transition zones at the Brunhes–Matuyama and upper Olduvai boundaries: preliminary results from ODP leg 104. Proc. Ocean Drill. Prog. Sci. Results 104, 903–910.

Singer, B.S., Pringle, M.S., 1996. Age and duration of the Matuyama–Brunhes geomagnetic polarity reversal from ^{40}Ar–^{39}Ar incremental heating analyses of lavas.

Sun, D., Shaw, J., An, Z., Rolph, T., 1993. Matuyama–Brunhes (M/B) transition recorded in Chinese loess. J. Geomagn. Geoelectr. 45, 319–330.

Tauxe, L., Herbert, T., Shackleton, N.J., Kok, Y.S., 1996. Astronomical calibration of the Matuyama–Brunhes boundary: consequences for magnetic remanence acquisition in marine carbonates and the Asian loess sequences. Earth Planet. Sci. Lett. 140, 133–146.

Theyer, F., Herrero-Bervera, E., Hsu, V., Hammond, S.R., 1985. The zonal harmonic model of polarity transitions: a test using successive reversals. J. Geophys. Res. 90, 1963–1982.

Turner, G.M., Kamp, P.J.J., 1990. Paleomagnetic location of the Jaramillo subchron and the Matuyama–Brunhes transition in the Castlecliffian stratotype section, Wanganui Basin, New Zealand. Earth Planet. Sci. Lett. 100, 42–50.

Valet, J.P., Meynadier, L., 1993. Geomagnetic field intensity and reversals during the past four million years. Nature 366, 234–238.

Valet, J.P., Tauxe, L., Clark, D.R., 1988. The Matuyama–Brunhes transition recorded from Lake Tecopa sediments (California). Earth Planet. Sci. Lett. 87, 463–472.

Valet, J.P., Tauxe, L., Clement, B., 1989. Equatorial and mid-latitude records of the last geomagnetic reversal from the Atlantic Ocean. Earth Planet. Sci. Lett. 94, 371–384.

Valet, J.P., Tucholka, P., Courtillot, V., Meynadier, L., 1992. Paleomagnetic constraints on the goemetry of the geomagnetic field during reversals. Nature 356, 400–407.

Zhu, R., Liu, C., Wu, H., Zhu, B., 1991. Transitional field behavior for the Matuyama–Brunhes. Sci. China Ser. B 34, 1252–1257, English translation.

Zhu, R., Ding, Z., Wu, H., Huang, B., Jiang, L., 1993. Details of magnetic polarity transition recorded in Chinese loess. J. Geomagn. Geoelectr. 45, 289–299.

Zhu, R., Laj, C., Mazaud, A., 1994. The Matayuma–Brunhes and Upper Jaramillo transitions recorded in a loess section at Weinan, north-central China. Earth Planet. Sci. Lett. 125, 143–158.